Rock and Soil Mechanics 2026 47(3): 793−815 ISSN 1000−7598
https: //doi.org/10.26599/RSM.2025.94300342 journal homepage: rocksoilmech.whrsm.ac.cn

Macro-micro properties of peaty soil stabilized with slag-based geopolymer and cement

SUN Yin-lei[1], LIAO Lei[1], ZOU Xi[1], ZHOU Yan-hua[2], CHENG Yun[2], GUO Yun-hao[1], WANG Zhi-liang[3], ZHANG Xian-wei[4]

1. School of Architecture and Planning, Yunnan University, Kunming, Yunnan 650500, China
2. YCIH No.1 Engineering Survey and Design Co., Ltd., Kunming, Yunnan 650000, China
3. Faculty of Civil and Architectural Engineering, Kunming University of Science and Technology, Kunming, Yunnan 650500, China
4. State Key Laboratory of Geomechanics and Geotechnical Engineering, Institute of Rock and Soil Mechanics, Chinese Academy of Sciences, Wuhan, Hubei 430071, China

Abstract: Peaty soil, a distinct category of soft foundation soil, exhibits unique physical and mechanical properties that are strongly influenced by its microstructure. Its high water content, organic matter content, low strength and permeability often result in significant engineering challenges. Enhancing the mechanical strength of peaty soil has thus become a central focus in geotechnical engineering. Using slag-based geopolymer to synergize with cement for solidification, the mechanical properties of peaty soil before and after stabilization were examined through unconfined compressive strength and direct shear tests. The mechanisms of improvement were further analyzed through microscopic techniques, including scanning electron microscope (SEM), X-ray diffraction (XRD), mercury intrusion porosimetry (MIP), and Fourier transform infrared spectroscopy (FTIR). The results demonstrate that all three alkali activators contribute to the enhancement of the mechanical strength of the peaty soil, with NaOH showing the highest activation efficiency. Cement stabilization of peaty soil improves shear strength by reducing pore space and strengthening interparticle bonding via ion exchange, hydration product crystallization, and the formation of $CaCO_3$ and calcium silicate hydrate (C-S-H). Four stages i.e., dissolution activation, ion exchange, gel formation, and structural reorganization are identified in the reaction process of activated slag improving peat soil. The alkali activator facilitates the dissolution of the slag's vitreous phase, promoting ionic polymerization that leads to the formation of calcium-alumino-silicate-hydrate (C-A-S-H) gel. Simultaneously, organic functional groups in the peaty soil engage in ion exchange, forming $CaSiO_3$ precipitates and establishing a "calcium bridge" structure. These reactions collectively contribute to the formation of a dense composite matrix, thus enhancing compressive strength. Grey relational analysis reveals that compressive strength is most strongly correlated with pore area, while shear strength shows the highest correlation with the shape factor. Modified soil specimens undergo five dry-wet cycles, with a minimum strength loss rate of 27%. These findings provide a theoretical foundation for the partial replacement of cement with alkali-activated slag in peaty soil stabilization, contributing both to soft soil improvement and the valorization of industrial byproducts. Furthermore, these results offer valuable insights for ground improvement in peat-rich regions, such as Yunnan, China.

Keywords: peaty soil; slag-based geopolymer; cement; mechanical strength; gray correlation method; microscopic mechanism

1 Introduction

Peaty soils are a distinctive type of soil formed by the incomplete decomposition of marsh plant remains in an oxygen-deprived, underwater environment, facilitated by anaerobic bacteria[1]. The presence of substantial undecomposed plant residues results in loose structures with well-developed porosity and generally poor physical and mechanical properties. Characterized by high organic matter content, elevated natural moisture, low natural density, and insufficient bearing capacity (the "two highs and two lows"), peaty soils are classified as special problem soils (soft soils) in engineering practice (Fig. 1)[2]. These soils are prone to engineering issues such as subgrade settlement and foundation cracking. Peaty soils derived from lacustrine sediments are widely distributed across the Dianchi Basin in Kunming, Yunnan[3−4]. With the advancement of large-scale infrastructure construction in the region, engineering projects inevitably involve such soil layers, and their treatment and improvement have become pressing practical issues that require urgent resolution[5].

Received: 7 June 2025 Accepted: 1 September 2025
This work was supported by the National Natural Science Foundation of China (52568054, 42372313, 42067043), the Natural Science Foundation of Yunnan Province, China (202401CF070174) and the Xingdian Talent Support Program (C619300A130).
First author: SUN Yin-lei, male, born in 1986, PhD, Associate Professor, focusing on soil dynamics and soil remediation. E-mail: sunylei@ynu.edu.cn
Corresponding author: ZHANG Xian-wei, male, born in 1982, PhD, Professor, focusing on basic research on special soil mechanics and applied research on disaster treatment. E-mail: xwzhang@whrsm.ac.cn

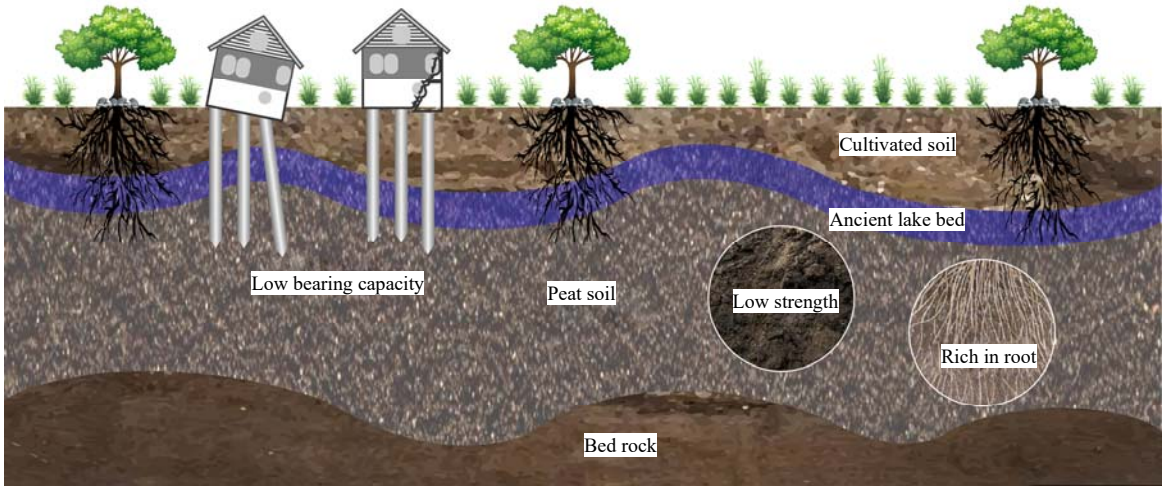

Fig. 1 Engineering defects of peaty soil

Numerous studies have been conducted globally on the consolidation and improvement of peaty soil. Kamaruidzaman et al.[6] partially replaced cement with sugarcane bagasse ash, significantly enhancing unconfined compressive strength while reducing porosity. Zaidan et al.[7] found that cement and ceramic dust improve consolidation properties. Kalantari et al.[8] highlighted the significant strength enhancement achieved through overloading and moist curing techniques. Rahman et al.[9] demonstrated that increasing cement content and curing age improves liquid limit and permeability. Wong et al.[10] replaced part of the cement with sodium-based bentonite, significantly boosting both compressive and shear strength. Latifi et al.[11] employed $MgCl_2$ solution curing to improve pore structure and enhance strength. Gui et al.[12] utilized microbial degradation of organic matter to significantly improve soil mechanical properties. Ruan et al.[13] achieved notable results with cement-lime-fly ash composite modification, validated by field testing. Cao et al.[14] emphasized the improvement in water resistance through the use of ultrafine cement. Wang et al.[15] investigated the effectiveness of frost heave control under artificial freezing conditions. These studies indicate that peat soil improvement primarily relies on chemical and biological methods, with cement being the most commonly used stabilizer.

Peaty soils, rich in organic matter and humic acids[16] significantly hinder cement hydration, diminishing the effectiveness of cement-based stabilization. Excessive cement content not only poses risks of shrinkage cracking but also leads to higher carbon emissions[17]. As a result, cement alone often fails to achieve optimal results and must be combined with other admixtures for effective curing. In recent years, geopolymers[18] have emerged as a novel eco-friendly cementitious material. Compared to cement-stabilized soft soil at equivalent dosages, geopolymers exhibit superior mechanical properties and lower carbon emissions[19–20], leading to their widespread use in engineering applications for soft soil reinforcement. Geopolymers are green cementitious materials formed by the reaction of precursors (such as blast furnace slag[21], fly ash[22], etc.) under alkaline activators. This technology has been successfully applied to marine soft soils[23], sludge[24], silty clays[25], and waste marine clay[26], achieving positive results. However, research on the application of alkali-activated slag for improving the properties of peat soil in the Dianchi Lake region remains limited, especially regarding its effects on the soil's strength, microstructure, and the underlying reinforcement mechanisms. Further studies are urgently needed in this area. Additionally, China's annual blast furnace slag output is projected to exceed 340 million tons by 2025, yet its utilization rate remains below 60%[27]. The partial substitution of cement with alkali-activated slag offers dual benefits: enhancing peat soil stabilization and promoting slag recycling, thus providing both economic and environmental advantages[28–29]. Geopolymer materials have demonstrated promising applications in engineering practices, including deep-mixing piles, grouting reinforcement, and contaminated soil solidification. Yao et al.[30] conducted stability analysis of geopolymer-mixed pile composite foundations through field tests, confirming that all indicators met specifications. Drilling, coring, and static load tests demonstrated the integrity of pile bodies, with both single-pile and composite foundations meeting design requirements. Sun et al.[31] explored geopolymer grouting for soft soil foundation treatment in highway construction, showing significant improvements in subgrade bearing capacity. In the Anhui Weijiu Road project, geopolymer grouting more than doubled the bearing capacity of the soil subgrade, yielding remarkable results. Pu et al.[32] experimented with a modified phosphate-based geopolymer composed of kaolinite, fly ash, and aluminum hydrogen phosphate, which effectively reduced Pb^{2+} leaching, significantly enhanced soil strength, and exhibited excellent acid resistance.

In summary, existing research has primarily focused on individual activators or solidification materials, with a lack of systematic studies on the synergistic solidification of peaty soils using alkali-activated slag and cement. Notably, the performance evolution under the combined effects of multiple factors-such as activator types and concentrations, as well as slag and cement dosages-remains unclear, along with the intrinsic relationship between microstructure and macroscopic mechanical properties. This study selected three alkaline activators -NaOH, Na_2CO_3, and Na_2SiO_3-and systematically analyzed their effects on the mechanical properties of composite solidified peaty soils using slag-based geopolymers and cement. Through scanning electron microscope (SEM), X-ray diffraction (XRD), mercury intrusion porosimetry (MIP), Fourier transform infrared spectroscopy (FTIR), and other microscopic techniques, the microstructure, mineral composition, and pore evolution characteristics of the solidified soils were investigated. Grey relational analysis was employed to quantitatively establish the correlation between microstructural parameters (e.g., pore number, area, shape factor) and macroscopic mechanical properties. Durability was assessed through dry-wet cycling tests. The study identified optimal solidification conditions for different activators and concentrations and revealed the evolution mechanisms of microstructure and pore characteristics within the alkali-activated slag-cement composite system at multiple scales. For the first time, grey relational analysis clarified the relationship between microstructure and mechanical properties, elucidating the full-process reaction mechanism of alkali-activated slag synergizing with cement to solidify peaty soils at a mechanistic level. The technical roadmap of study is shown in Fig. 2.

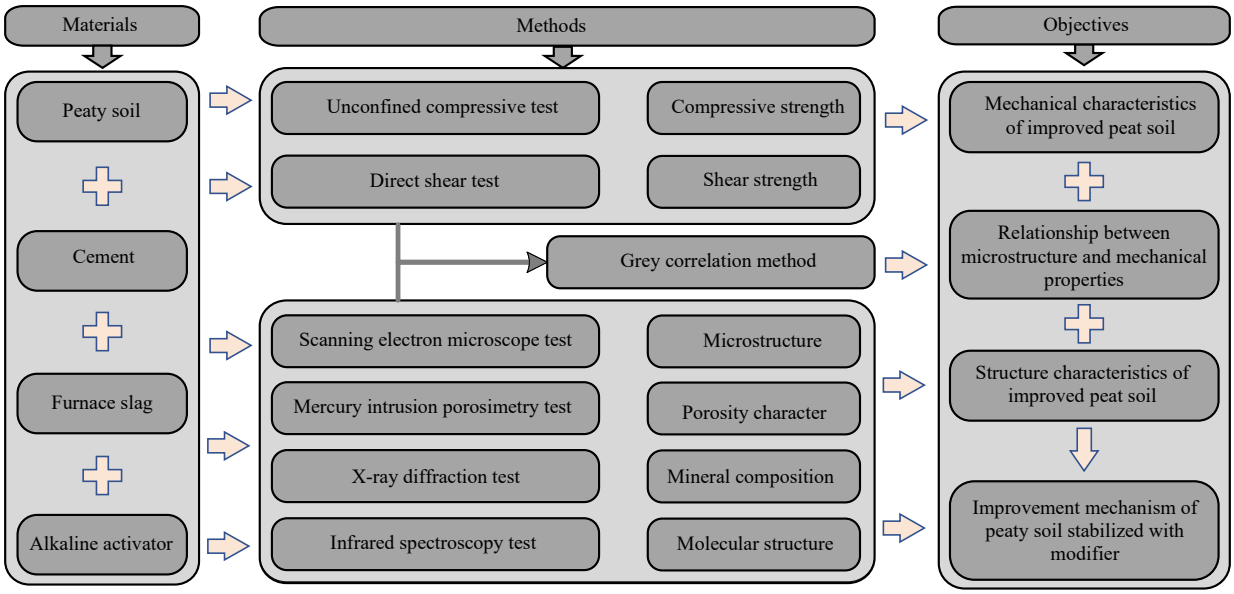

Fig. 2 Technical roadmap

2 Experimental materials and methods

2.1 Experimental materials

The peat soil used in this study was collected from a construction site near the Dianchi Convention and Exhibition Center in Kunming, Yunnan Province. The in-situ soil exhibited a black to gray-black appearance, a light texture rich in organic matter, a loose structure with a large pore ratio, and a soft, fluid-plastic consistency characterized by high water content. Its fundamental physical properties, including natural water content, liquid limit, and plastic limit, were determined in accordance with the organic soil testing standards[33], as summarized in Table 1. The cement(C) utilized in this study was type P.O 42.5, while the furnace slag (FS) was sourced from a steel plant in Kunming. The slag was ground granulated blast furnace slag powder, composed of fine, irregular particles. Its main chemical components included Fe_2O_3, CaO, SiO_2, and Al_2O_3, as well as trace amounts of Mg, Na, and other elements, which endows it with a certain chemical reactivity. The NaOH, Na_2CO_3, and Na_2SiO_3 employed in the experiments were obtained from a chemical reagent manufacturer in Kunming, with a purity of industrial analytical grade.

Table 1 Physico-mechanical properties of peaty soil

Natural moisture content w /%	Natural density ρ/(g • cm^{-3})	Porosity ratio e	Organic matter content w_u /%	Liquid limit w_L /%	Plastic limit w_P /%	Cohesive force c/kPa	Angle of internal friction φ/(°)	Unconfined compressive strength q_u /kPa
192.9	1.48	4.56	34.5	57	35	16.3	5	195

2.2 Sample preparation

This test employed the static pressure method for soil sample preparation, with the optimum moisture content determined to be 43% based on the percussion test. The baseline dosage of slag powder was set at 20%, and three types of alkaline activators (NaOH, Na_2CO_3, and Na_2SiO_3) were selected for comparison. Preliminarily, cement and slag with different dosages were added individually for preliminary tests. Orthogonal experiments were subsequently conducted with cement dosages of 5%, 7%, 10%, and 12%, and slag dosages of 10%, 20%, and 30%. Based on these results, the optimal combination of cement and slag was determined, and subsequent tests were conducted using three different concentrations of alkali activators.

Prior to specimen preparation, the collected peaty soil was crushed and sieved through a 2 mm mesh. Due to its high organic matter and moisture content, elevated temperatures could lead to the decomposition of organic matter and rapid water loss from soil particles, potentially damaging the microstructure and adversely affecting the mechanical properties. To mitigate this, the soil was oven-dried at 65 ℃ for 24 hours until a constant weight was achieved. In accordance with the experimental protocol, predetermined amounts of dried peat soil, cement, and slag were weighed and thoroughly mixed by a small indoor mixer. The pre-weighed water and the three activators were successively added to a beaker, stirred thoroughly with a glass rod, and allowed to dissipate heat. The prepared alkaline solution was then added to the dry soil-slag and dry soil-cement-slag mixtures, which were mixed uniformly for 5 minutes before molding the specimens. Specimens were prepared using a layered compaction method to produce cylindrical compressive specimens (ϕ50 mm × 50 mm) and shear specimens (ϕ61.8 mm × 20 mm). A uniform maximum dry density of 0.967 g/cm³ was adopted, with three parallel specimens prepared for each group. Based on the findings of Consoli[34] and Sariosseiri[35], modified soil samples containing Portland cement (P.O 42.5) typically achieve the strength of most cements within 7 days. Accordingly, the specimens were demolded, wrapped in plastic film, sealed, and placed in a standard curing chamber (20±1 ℃, 90%±1% relative humidity) until the target curing age of 7 days was reached, after which unconfined compressive strength and direct shear tests were performed[36]. The experimental setup diagram of this paper is shown in Fig. 3.

2.3 Experimental methods

2.3.1 Unconfined compressive strength test

After curing the specimens to the specified age, unconfined compressive strength (UCS) testing was performed using a WDW-50 electronic universal testing machine. Prior to the tests, the two ends of the specimens were trimmed to be flat and centered in the loading device to ensure uniform stress distribution across the specimen. During the test, axial monotonic loading was applied at a constant rate of 1 mm/min, with axial load and deformation monitored in real time. The test was terminated when the stress-strain curve reached its peak and then stabilized; if no obvious

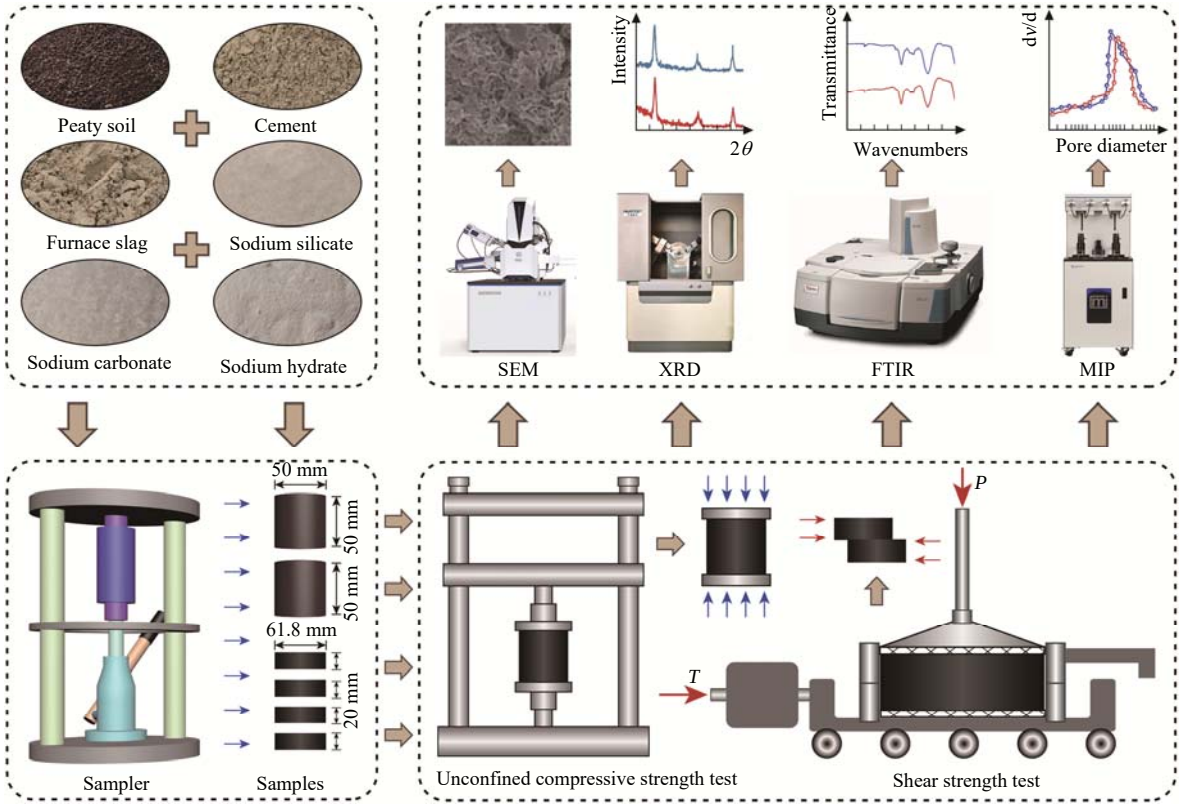

Fig. 3 Test device diagram

peak failure was observed, the test was stopped when the axial strain reached 20%. The unconfined compressive strength was determined by dividing the maximum load by the specimen's initial cross-sectional area.

2.3.2 Direct shear test

This study adopted a ZJ-type strain-controlled four-shear apparatus, manufactured by the Nanjing Soil Instrument Factory, to carry out the direct shear tests. After being cured to the designated curing age, the specimens were placed into the shear boxes, aligned, and fixed in the upper and lower shear boxes along the horizontal shear plane. Normal stresses of 100 kPa, 200 kPa, 300 kPa, and 400 kPa were applied incrementally, with constant normal stress maintained throughout loading. Shear was controlled by strain at a constant rate of 0.8 mm/min. Shear stress and displacement were recorded in real time during the test. The shear strength parameters were determined based on shear stress at various normal stresses. The test was terminated when the shear force peaked and began to decline, or when the shear displacement reached the specified range. The shear stress during the process was calculated using the following equation:

$$\tau = \frac{C \cdot R}{A_0} \times 10 \tag{1}$$

where τ is shear stress (kPa), C is calibration coefficient of the dynamometer (N/0.01 mm), A_0 is cross-sectional area of the specimen (cm^2), R is dynamometer reading (0.01 mm).

2.3.3 Scanning electron microscope (SEM)

In this study, the microstructure of the samples was examined using a Zeiss Sigma 300 scanning electron microscope (SEM). Magnifications of 1.0k, 5.0k, 10.0k, and 50.0k were employed to perform a comprehensive analysis of the micromorphological characteristics. To ensure the representativeness and reliability of the results, each micro specimen was examined at a minimum of five randomly selected scanning points. To further investigate the microstructure and particle arrangement of the peat soil, the scanning electron microscopy (SEM) images were quantitatively analyzed by the Particle and Crack Analysis System (PCAS), which applies the grey relational analysis method and incorporates parameters such as shape factor, pore length, pore area, and correlation coefficient for microstructural evaluation.

2.3.4 X-ray diffraction (XRD)

Samples from representative fracture surfaces of soil specimens subjected to compressive or shear testing were collected for mineralogical composition analysis. The specimens were pulverized, passed through a 0.25 mm sieve, and prepared as flat sections with a thickness ranging from 1.0 to 2.0 mm. The mineralogical composition was determined by a Bruker D8 Advance X-ray diffractometer (XRD), with the test parameters as follows: a scanning range of 5°–90°, a scanning rate of 2.000°/min, a sampling step of 0.02°, and a counting time of 0.12 s.

2.3.5 Mercury intrusion porosimetry (MIP)

Mercury intrusion porosimetry was employed to characterize the soil microstructure, including pore size and distribution. In this study, an Auto Pore IV 9510 fully automated mercury porosimeter was used to perform the measurements. Soil specimens were cut into small cubes approximately 2−3 mm in size, immersed in isopropyl alcohol, freeze-dried, and subsequently subjected to MIP analysis. The maximum applied mercury pressure was 60 000 psi(1 psi≈6 894.757 Pa), with a minimum detectable pore diameter of 3.02 nm, and a mercury-specimen contact angle of 130°.

2.3.6 Fourier transform infrared spectroscopy (FTIR)

Fourier transform infrared spectroscopy (FTIR) was performed using a Bruker ALPHA II instrument to assess variations in soil organic matter content. Soil samples were dried to a constant weight, ground into a fine powder, and sieved through a 0.075 mm mesh. A measured amount of powder was then placed onto a diamond ATR crystal and subjected to constant pressure. The infrared absorption wavenumber range was 4 000−400 cm^{-1}, with the attenuated total reflection (ATR) range spanning 4 000−525 cm^{-1}.

3 Results and analysis

3.1 Unconfined compressive strength

3.1.1 Single and double blended improvers

Fig. 4 presents the unconfined compressive strength test results for soils modified with cement, slag, and their mixtures. As shown in Fig. 4(a), the maximum stress of the peat soil increases with the increase in cement content. At 5% cement, the maximum stress reaches approximately 150 kPa, while at 15% cement, it increases to 550 kPa, highlighting the significant role of cement in strengthening the soil. After reaching maximum stress, the curve slightly declines, and the higher the cement content, the later the peak stress occurs, indicating that the soil can sustain greater deformation without failure. Fig. 1 shows a steady increase in the stress values with the increase in cement content, Fig. 2 reveals a positive correlation between the stress values and slag content, with an overall increase of 330 kPa, reflecting a substantial strengthening effect. In contrast, Fig. 4(b) shows that although soil strength increases with higher slag content, the overall magnitude is much lower than that of cement, with a maximum value of only 376 kPa. Fig. 2 indicates a positive correlation between stress values and slag content, but the trend is relatively flat, suggesting that slag's effect on strength enhancement is limited.

After blending cement and slag in varying ratios, tests were conducted. As shown in Fig. 4(c), increasing slag content led to a curve characterized by an initial rise followed by a decline. However, due to the influence

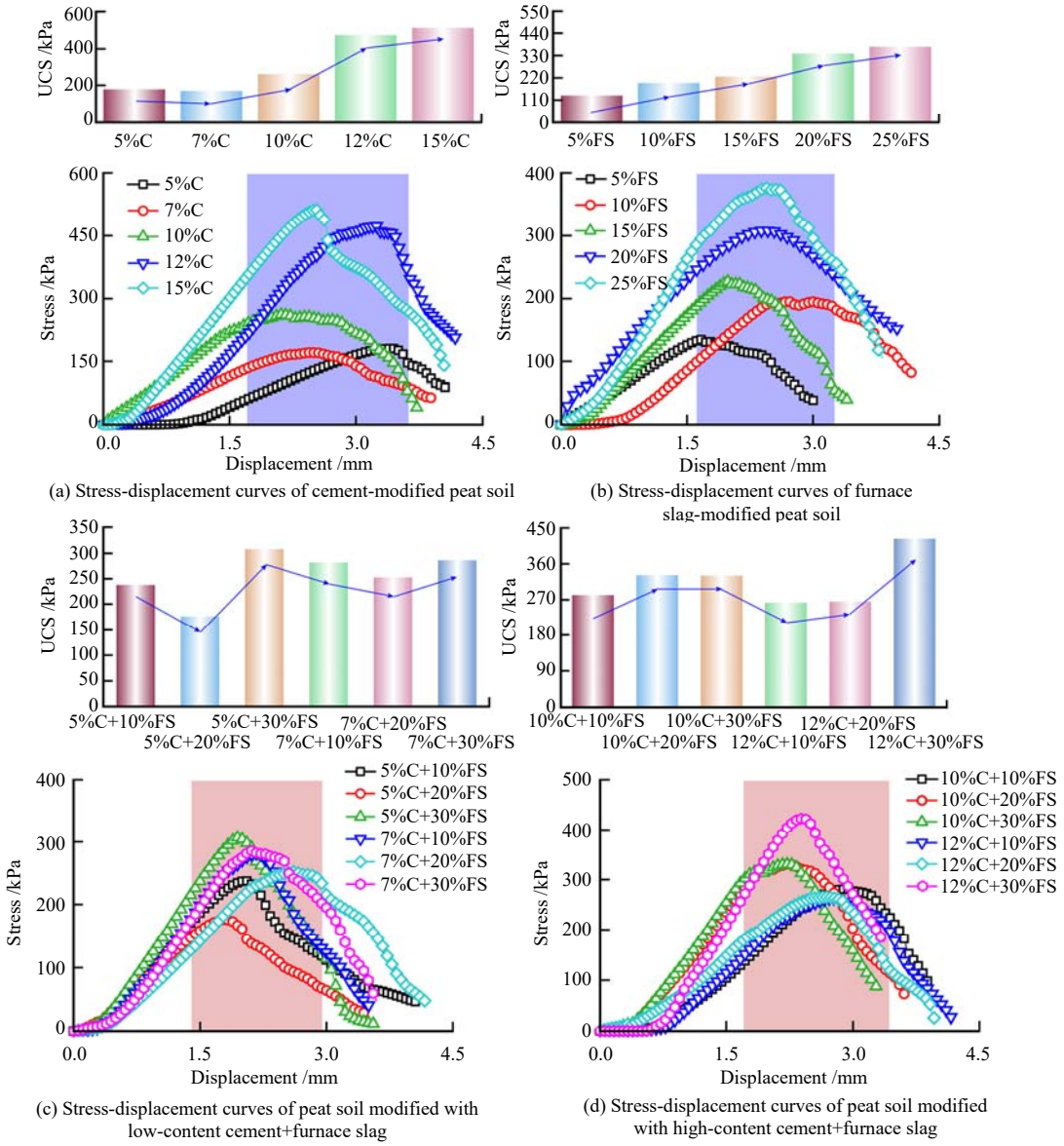

(a) Stress-displacement curves of cement-modified peat soil

(b) Stress-displacement curves of furnace slag-modified peat soil

(c) Stress-displacement curves of peat soil modified with low-content cement+furnace slag

(d) Stress-displacement curves of peat soil modified with high-content cement+furnace slag

Fig. 4 Stress-displacement curves of single and compounded modifiers

of slag, the curve dropped more significantly beyond 2 mm of displacement. The bar chart indicates a slight increase in stress at lower slag content, followed by a decrease as the slag proportion increases. At a cement-to-slag ratio of 5% to 10%, the maximum stress reaches approximately 250 kPa, whereas it drops to 150 kPa at 20% slag content. A similar trend is observed at 7% cement, with both cement ratios showing an inflection point at 20% slag. Fig. 4(d) demonstrates that stress growth slows with increasing slag content, and the curve flattens after displacement exceeds 2 mm, resulting in a significant decrease in compressive strength. The results in Fig. 4 show that the 10% cement ratio yields higher compressive strength, while excessive cement or slag reduces the improvement effect. In summary, cement effectively enhances soil compressive strength, whereas slag alone has limited impact, and excessive slag diminishes strength. Orthogonal experiments indicate that the optimal mix ratio is 10% cement and 20% slag.

3.1.2 Slag + alkali activator

Fig. 5 presents the stress-displacement curves from unconfined compressive strength tests on specimens treated with various alkali activators. Regardless of concentration or slag dosage, NaOH(NH) exhibited the most significant activation effect, which significantly improved the compressive strength of the peat soil. At slag dosages of 10% and 20%, combined with alkali concentrations of 7% and 9%, the soil achieved a higher peak strength at approximately 4.5 mm displacement, indicating increased rigidity. The corresponding maximum stress exceeded 1 MPa, meeting practical engineering requirements. In contrast, Na_2CO_3(NC) showed a weaker activation effect, producing lower peak stress and a modest curve increase, indicating limited improvement in strength. The activation effect of Na_2SiO_3(NS) was even milder, with lower peak stresses compared to NaOH and a more rapid stress decline with increasing displacement, suggesting weaker activation. Overall, NaOH had the most pronounced

effect on enhancing soil strength, especially at 10% and 20% slag dosages. At concentrations of 3%, 5%, and 7%, Na_2SiO_3 exhibited a stronger activation effect than Na_2CO_3, while at 9% concentration, Na_2CO_3 outperformed Na_2SiO_3. Furthermore, increasing slag dosage generally enhanced soil strength; however, for Na_2CO_3 and Na_2SiO_3, a 30% slag content reduced the strengthening effect.

The stress-displacement curves, obtained from unconfined compressive strength tests on specimens treated with varying concentrations of alkali activators, are shown in Fig. 6. As illustrated, stress values under NaOH activation increased significantly with higher concentrations, with the most pronounced improvement observed at elevated alkali concentrations combined with blast furnace slag addition. In Fig. a-1, b-1, and c-1, NaOH demonstrated the most substantial enhancement effect. Notably, the curve increased most rapidly under the combined action of 30%FS + 9%NaOH, with the maximum stress rising sharply to 1 881.33 kPa. The peak occurred at a lower displacement, indicating that the soil achieved higher compressive strength with reduced deformation. In contrast, Na_2CO_3 showed a relatively weak activation effect. While stress values increased with rising Na_2CO_3 concentrations, the improvement was substantially lower than that achieved with NaOH. In Fig. a-2, b-2, and c-2, the stress-displacement curves exhibited a more gradual rise, and the maximum stress values remained relatively low. Even at a concentration of 9%, the curves increased

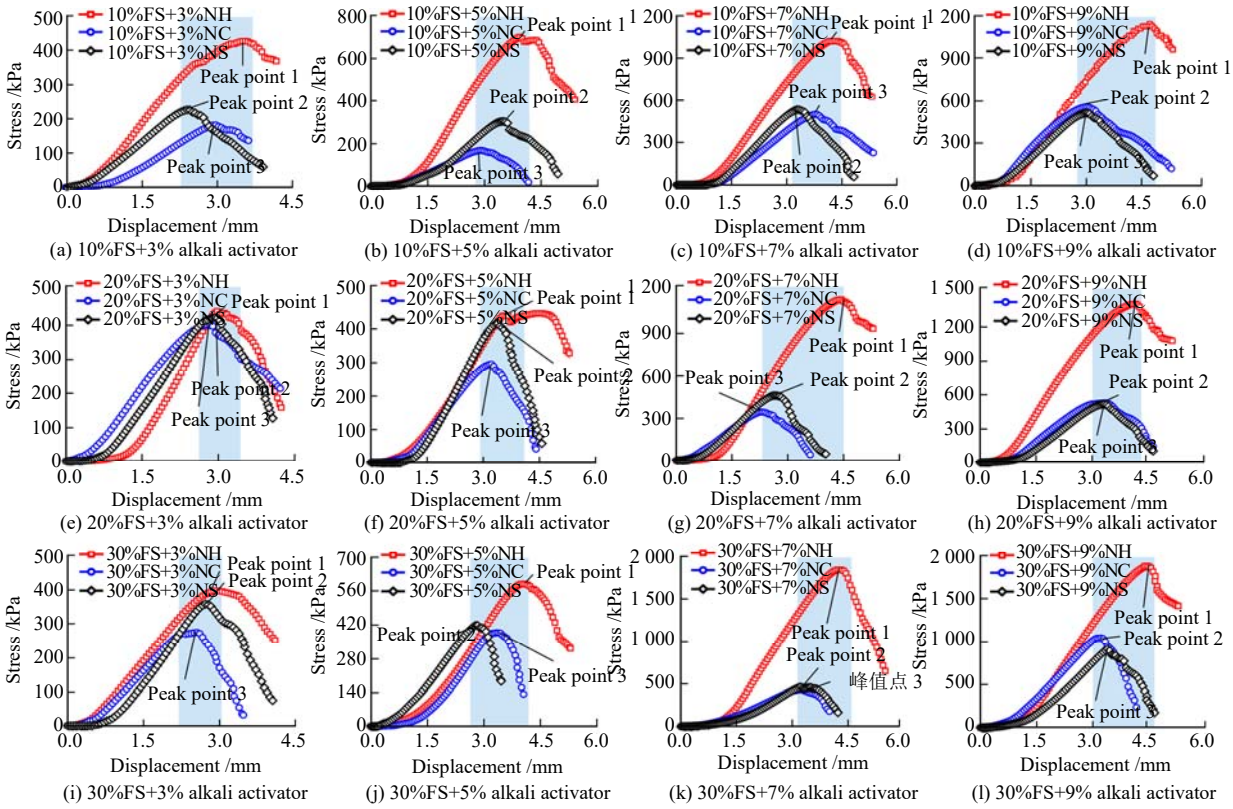

Fig. 5 Stress-displacement curves of peaty soil treated using different types of alkali activators

at a much slower rate compared to those of NaOH.

The activation effect of Na_2SiO_3 was comparatively moderate. While stress values increased with higher concentrations, its effect was more limited than that of NaOH and Na_2CO_3. Notably, even at a concentration of 9%, the increase in stress was less pronounced than that observed with NaOH. The data indicated that, at a slag dosage of 30%, the activation effect of Na_2SiO_3 was inferior to the other two alkali activators. Overall, increasing the activator concentration significantly enhanced its activation effect. The compressive strength of the soil showed a positive correlation with NaOH concentration, with stress values rising substantially as the concentration increased, reaching its most pronounced effect at 9%. While higher concentrations of Na_2CO_3 and Na_2SiO_3 also enhanced compressive strength, their effects were considerably weaker than those of NaOH, particularly at higher concentrations. The extent of improvement with these two activators was significantly lower compared to NaOH.

The compressive stress-displacement curves revealed that, regardless of slag dosage, specimens treated with higher concentrations of NaOH (7% and 9%) consistently exhibited superior compressive strength, with maximum stress values surpassing 1 MPa, confirming NaOH's superior activation efficiency compared to the other two activators (Fig. 7). Additionally, under high-concentration NaOH, the peak stress occurred later in the curve, at a

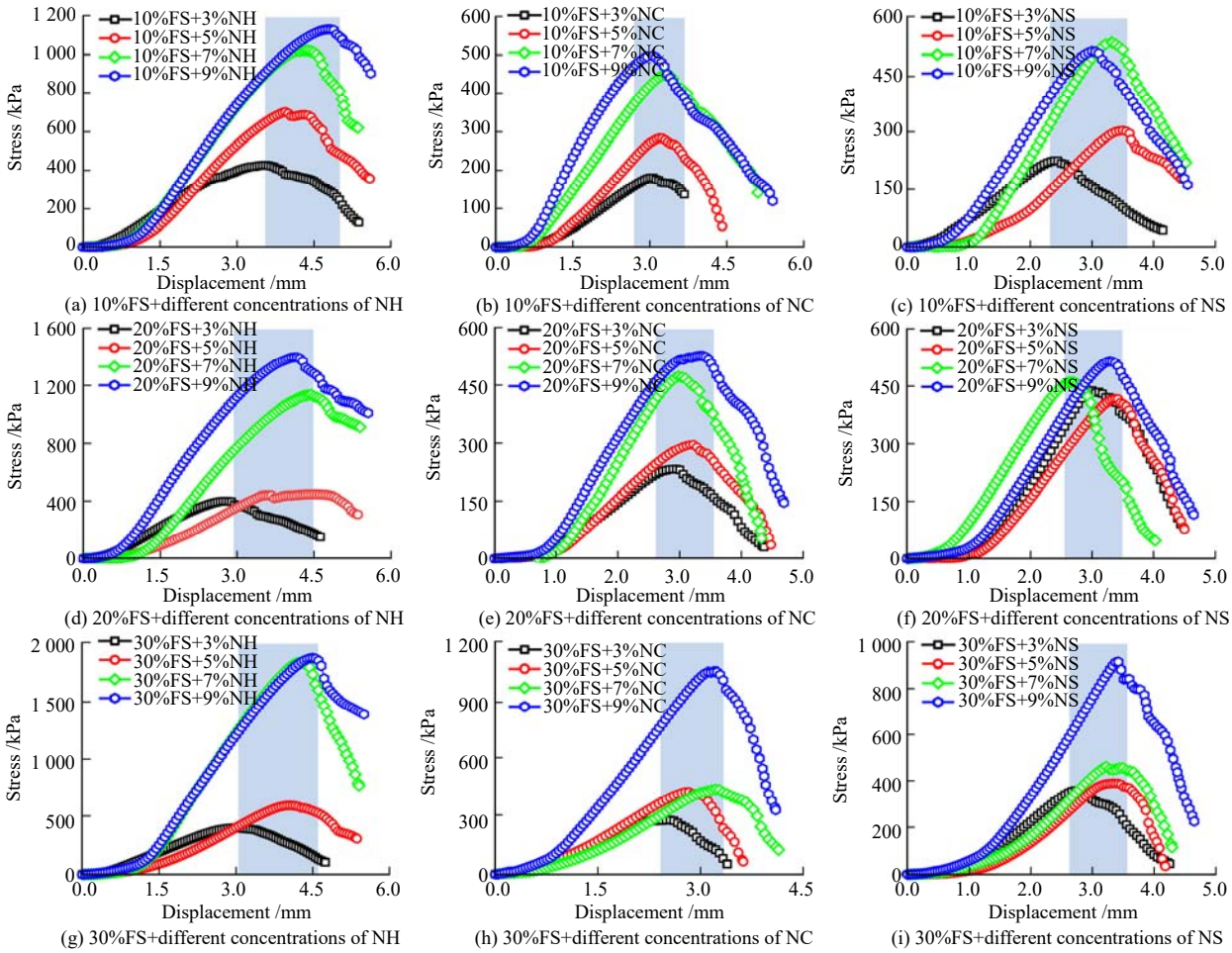

Fig. 6 Stress-displacement curves of peaty soil treated using different concentrations of alkali activators

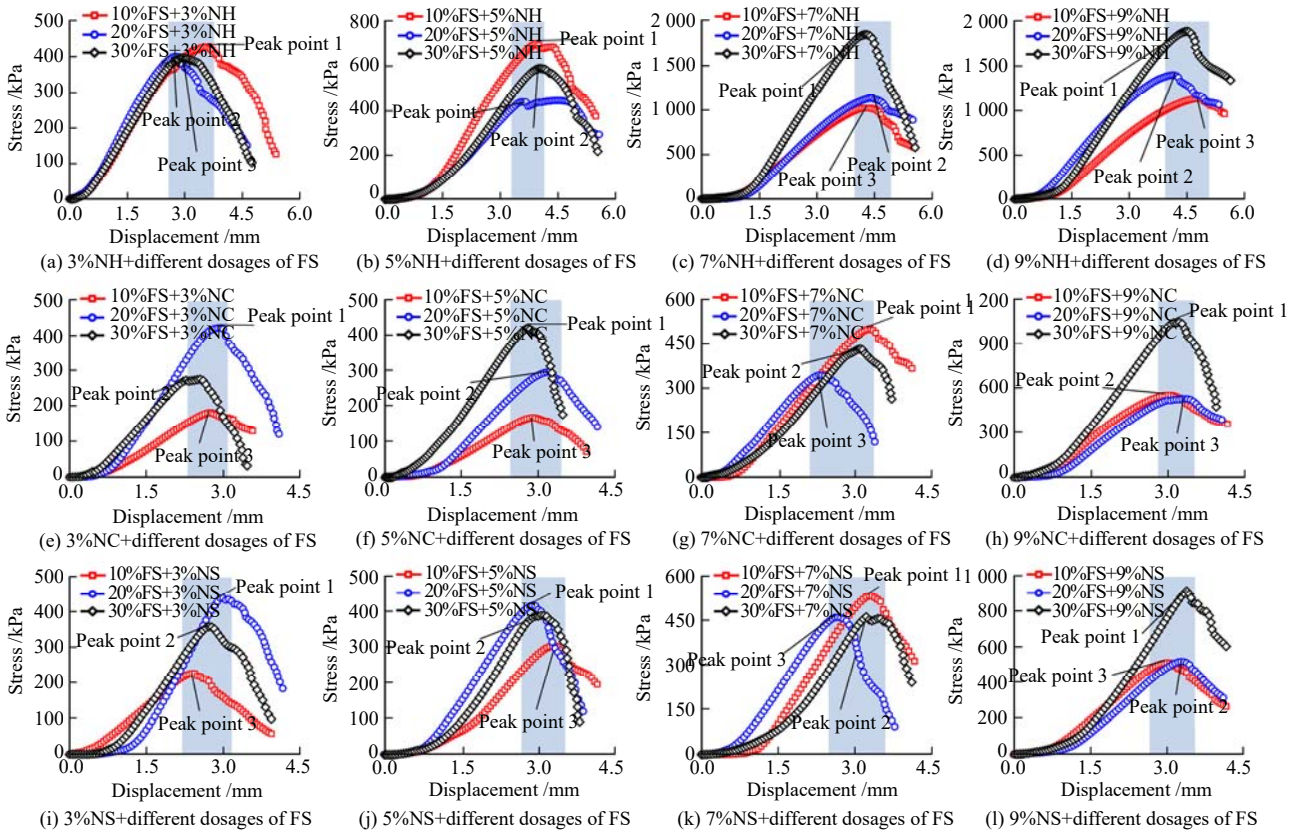

Fig. 7 Stress-displacement curves of peaty soil treated at different slag dosages

displacement of 4.5 mm, whereas for other slag-activator combinations, the peak typically appeared around 3 mm. For each activator, an overall increase in stress response was observed with higher slag content. However, at a 3% activator concentration, both Na_2CO_3 and Na_2SiO_3 showed reduced activation efficiency when the slag dosage reached 30%.

Overall, increasing slag content improved the compressive strength of the soil, with more pronounced enhancements observed at higher dosages (20% and 30%). The addition of 30% slag resulted in the most significant strength improvement, particularly when combined with NaOH, leading to a substantial increase in compressive strength. A 20% slag dosage exhibited a more balanced performance, yielding moderate strength improvements across different alkali activators. Specifically, the 20% slag dosage produced a balanced enhancement under various alkali activators, moderately increasing both compressive strength and maximum stress, though the effect was less pronounced than with the 30% dosage. At a 10% slag dosage, the activation effect was relatively modest; while alkali activators still influenced the soil, overall compressive strength was lower, and the stress-displacement curve displayed a gentler slope.

3.1.3 Cement + slag + alkali activator

Fig. 8 presents the stress-displacement curves from unconfined compressive strength tests on specimens containing 10% cement and 20% slag, subjected to different activators at varying concentrations. As shown in Fig. 8(a) and 8(b), at lower activator concentrations, the curve rises most rapidly when Na_2CO_3 is used. As concentration increases, the peak stress point shifts later, indicating enhanced compressive resistance. Fig. 1 and 2 reveal that Na_2CO_3 exhibits superior activation effects compared to the other two activators, achieving a maximum stress of 1 333.34 kPa at a 5% concentration. As concentrations increased to 7% and 9%, Fig. 3 and 4 demonstrate that NaOH provided the best activation effect, with compressive strengths exceeding 1 MPa. Additionally, 9% Na_2CO_3 and Na_2SiO_3 also achieved activation effects surpassing 1 MPa. In Fig. 8(c) and 8(d), the NaOH-treated curve showed the fastest rate of increase, while the peak stress points for all three curves continued to shift to later stages. Fig. 8(e), 8(f), and 8(g) explore the effects of varying concentrations of the same activator. Overall, the peak points for all curves occur around a 3 mm displacement.

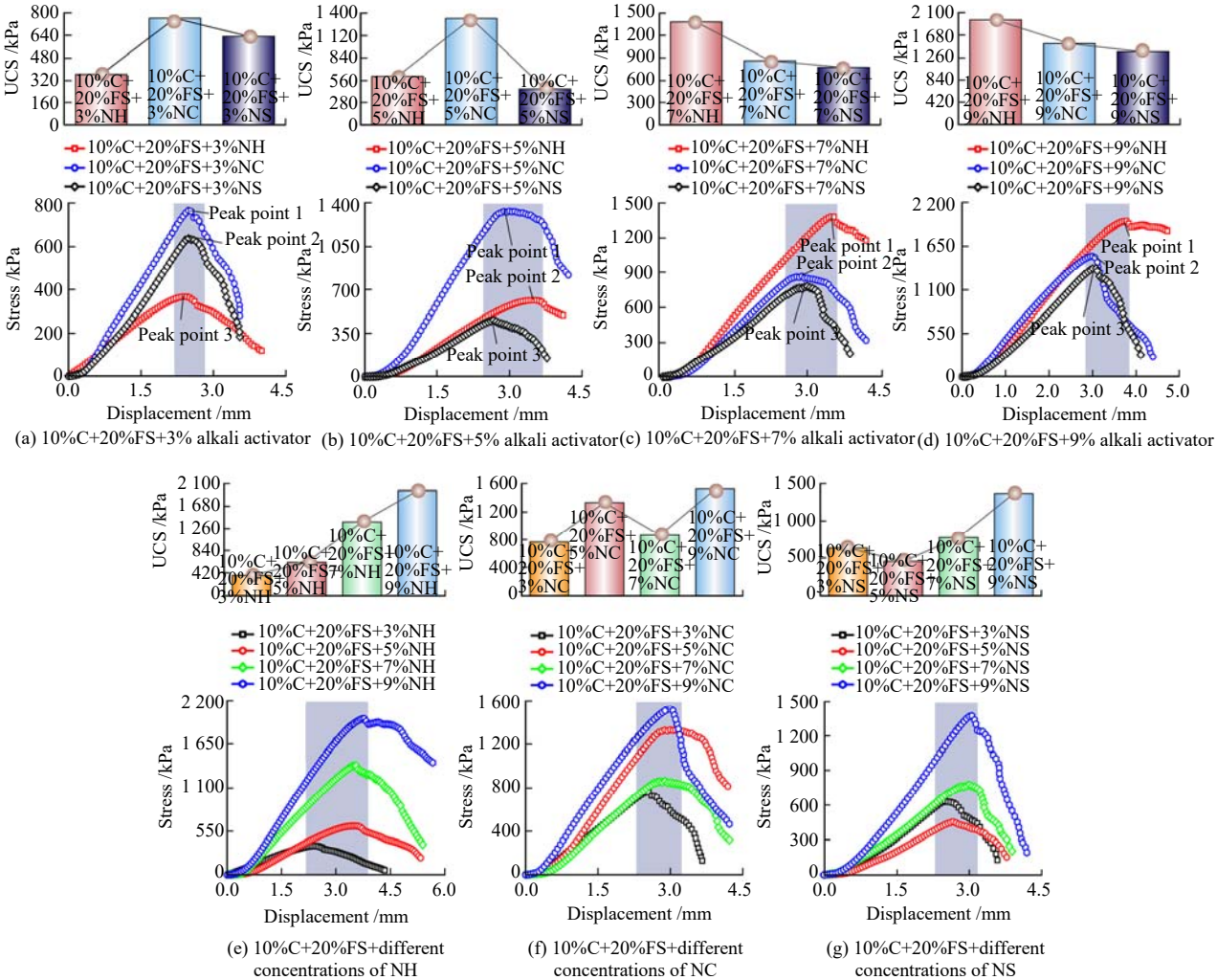

Fig. 8 Stress-displacement curves of peaty soil treated using different types and concentrations of alkali activators

At higher concentrations, the curves show a faster rate of increase, with stress values further elevated. The accompanying bar charts indicate that NaOH has the most pronounced activation effect, with stress values gradually rising with concentration, reaching a maximum of 1 967 kPa. The other two activators follow similar trends. Although the maximum stress in the treated soil increases with concentration for both Na_2CO_3 and Na_2SiO_3, their effects are comparatively milder, exhibiting smaller increments in stress compared to NaOH.

Fig. 9 illustrates the failure process of soil specimens during unconfined compressive strength testing. Due to the limited activation effect at low alkali concentrations, only failure processes under high-concentration conditions are analyzed. As shown in Fig. 9(a), the specimen maintained good integrity during the initial loading phase. With increasing pressure, oblique shear cracks gradually formed, eventually leading to a major rupture, indicative of significant shear failure. After failure, the specimen fragmented into larger pieces, retaining some structural integrity. At a NaOH concentration of 9%, the specimen exhibited greater overall integrity, with crack propagation slowing (Fig. 9(b)). The failure was characterized by enhanced plastic deformation and a more uniform crack distribution, with the specimen fracturing into larger, partially intact fragments. In Fig. 9(c), the specimen maintained initial integrity, followed by axial splitting during failure. Cracks propagated vertically, causing partial spalling of the specimen. After failure, longitudinal cracks were more prevalent, but the specimen retained a substantial residual structure. Fig. 9(d) shows that increasing concentration improved specimen integrity, with cracks propagating more slowly and in fewer numbers. The failure mode shifted from axial splitting to more stable crack development, resulting in a more ductile behavior. As shown in Fig. 9(e), specimens initially exhibited integrity, but rapid crack propagation and spalling occurred upon failure. Following damage, extensive fragmentation and spalling led to a loss of integrity, reflecting pronounced brittle failure characteristics. With increasing concentration (Fig. 9(f)), crack propagation slowed, and the failure pattern improved slightly. Despite the increase in Na_2SiO_3 concentration, the specimens continued to exhibit brittle failure, with rapid fragmentation following crack propagation.

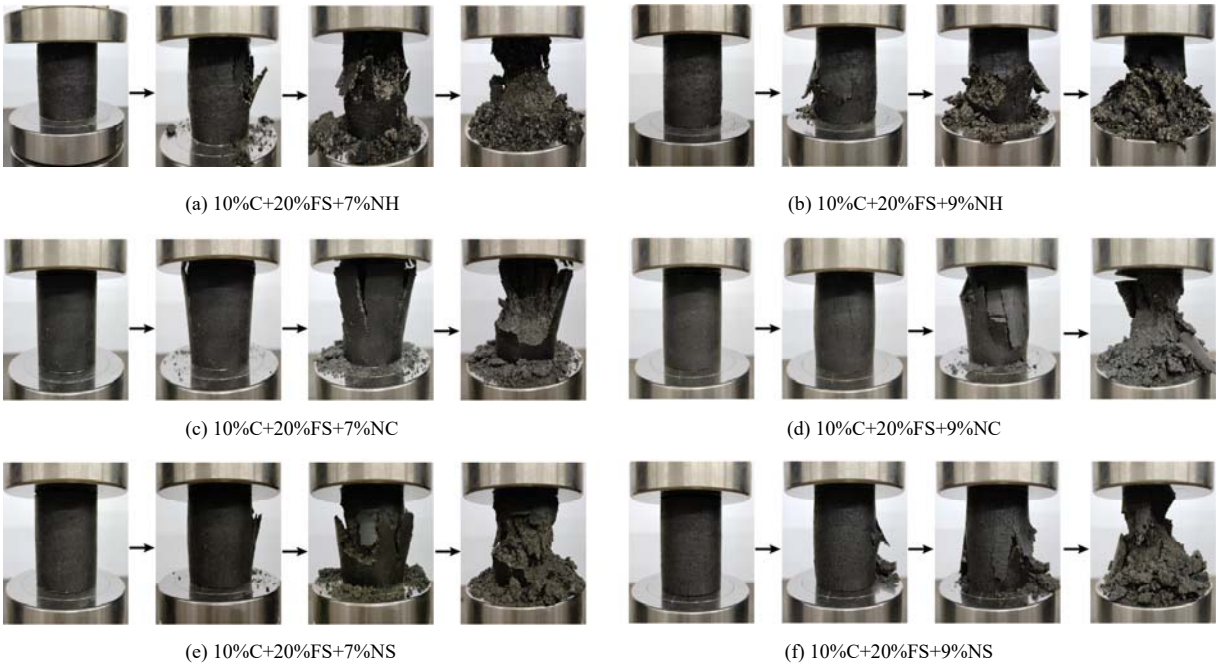

Fig. 9 Destruction processes of soil samples observed in unconfined compressive strength tests

3.2 Shear strength

3.2.1 Relationship between stress and displacement

The incorporation of various alkali activators at different concentrations into a mixture of 10% cement and 20% slag significantly enhances the shear strength of soil specimens, with the resulting curves displaying characteristics of brittle failure, most notably under NaOH activation. Taking NaOH as an example, Fig. 10 presents the shear stress-displacement curves for soil specimens subjected to different vertical stresses, along with their corresponding cohesion (c) and internal friction angle (φ) values. As evident from the figure, all curves show a distinct peak shear stress, initially increasing to a maximum before rapidly declining, which is indicative of brittle failure. The residual strength after failure remains low, with shear stress decreasing and stabilizing at a level significantly lower than the peak. Moreover, as vertical stress increases, peak shear stress correspondingly rises; however, at higher vertical stresses, the post-peak drop in shear stress becomes more pronounced, with curves

declining at an accelerated rate. Fig. 10(a) to 10(d) (uncemented) and 10(e) to 10(h) (cemented) show that peak shear stress increases with higher NaOH concentrations. Cement-stabilized specimens exhibit considerably higher peak shear stresses compared to uncemented specimens, especially under higher vertical stress conditions. The shear stress curves of uncemented specimens demonstrated a gradual increase in stress with relatively good ductility under vertical stresses of 100 kPa and 200 kPa, followed by a slow decline after reaching peak shear stress. In contrast, cement-stabilized specimens exhibited steeper curves, lower ductility, and more pronounced stress drops, particularly under vertical stresses of 300 kPa and 400 kPa, where peak shear stress was reached more quickly. The shear stress rapidly peaked before sharply declining, exhibiting a more pronounced brittle failure mode.

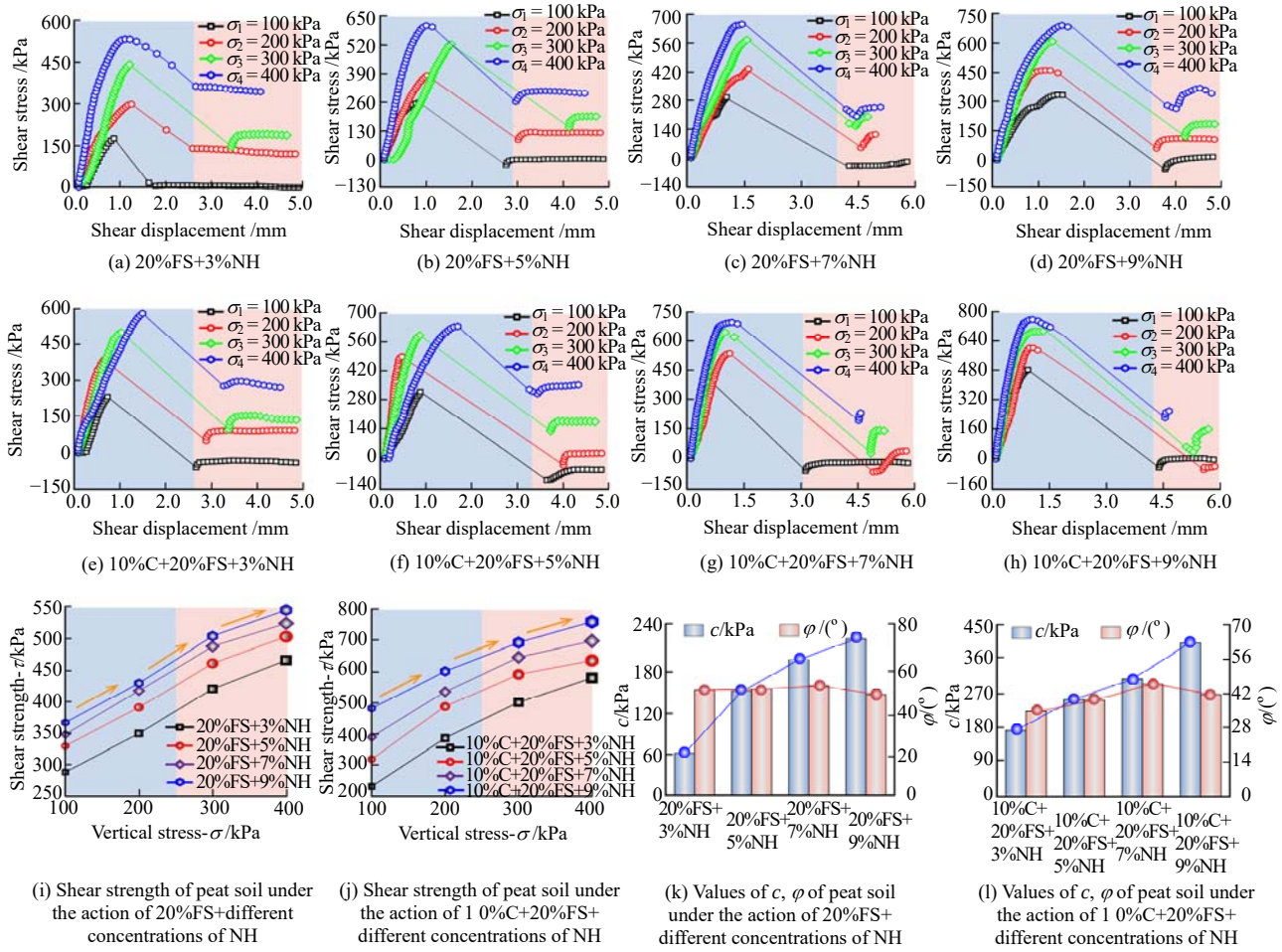

Fig. 10 Shear stress versus displacement curves for soil samples treated with NaOH, and the corresponding shear strength parameters (*c* and *φ*)

In Fig. 10(i), shear strength increases with rising normal stress, consistent with the Mohr-Coulomb strength criterion. As NaOH concentration increases, the soil's shear resistance under varying normal stresses is further enhanced. Following cement addition, the overall shear strength of the soil increases due to cement hydration and cementation (Fig. 10(j)). Notably, the soil treated with 9% NaOH demonstrated strong shear resistance under different normal stresses. The results for cohesion and internal friction angle showed that, without cement, cohesion increased with NaOH concentration, while the internal friction angle initially rose and then decreased. After cement addition, cohesion continued to increase, while the internal friction angle displayed a trend similar to that in Fig. 10(k). Overall, the modifier significantly enhanced soil cohesion, and the internal friction angle increased relative to the untreated sample, although the trend was more gradual. Under 7% NaOH treatment, both cohesion and internal friction angle reached relatively high values, while the internal friction angle under 9% NaOH showed a slight decrease.

3.2.2 Changes in shear strength indicators

Fig. 11 presents the cohesion and internal friction angle values for soil samples treated with different types and concentrations of alkali activators. The results show that, across all mixtures, NaOH-treated samples exhibited superior shear resistance, with cohesion reaching a maximum of 403.6 kPa. Without cement addition, cohesion initially

decreased and then increased at the same alkali activator concentrations, with Na_2CO_3 resulting in the lowest cohesion values. The internal friction angle generally decreased, although the variation was less pronounced than that of cohesion. After cement addition, cohesion gradually decreased, with the lowest value observed under Na_2SiO_3 treatment. In contrast, the internal friction angle initially increased and then decreased, peaking under Na_2CO_3 treatment.

For soil samples without cement addition, cohesion values increased significantly as the activator concentration rose from 3% to higher levels; however, this upward trend plateaued after cement addition. Under NaOH treatment, cohesion increased with concentration. Both cohesion and internal friction angle values initially increased and then decreased, both before and after cement addition, with the optimal enhancement observed at a 7% concentration. The effect of Na_2CO_3 also strengthened progressively with increasing concentration. After cement addition, cohesion values increased significantly, while changes in the internal friction angle were relatively gradual. Compared to Na_2CO_3, Na_2SiO_3 treatment generally resulted in lower internal friction angle values. Without cement, Na_2SiO_3 produced higher cohesion values than Na_2CO_3, with a more pronounced upward trend. After cement addition, Na_2CO_3 yielded higher cohesion values than Na_2SiO_3, with changes in the internal friction angle under both activators being relatively gradual.

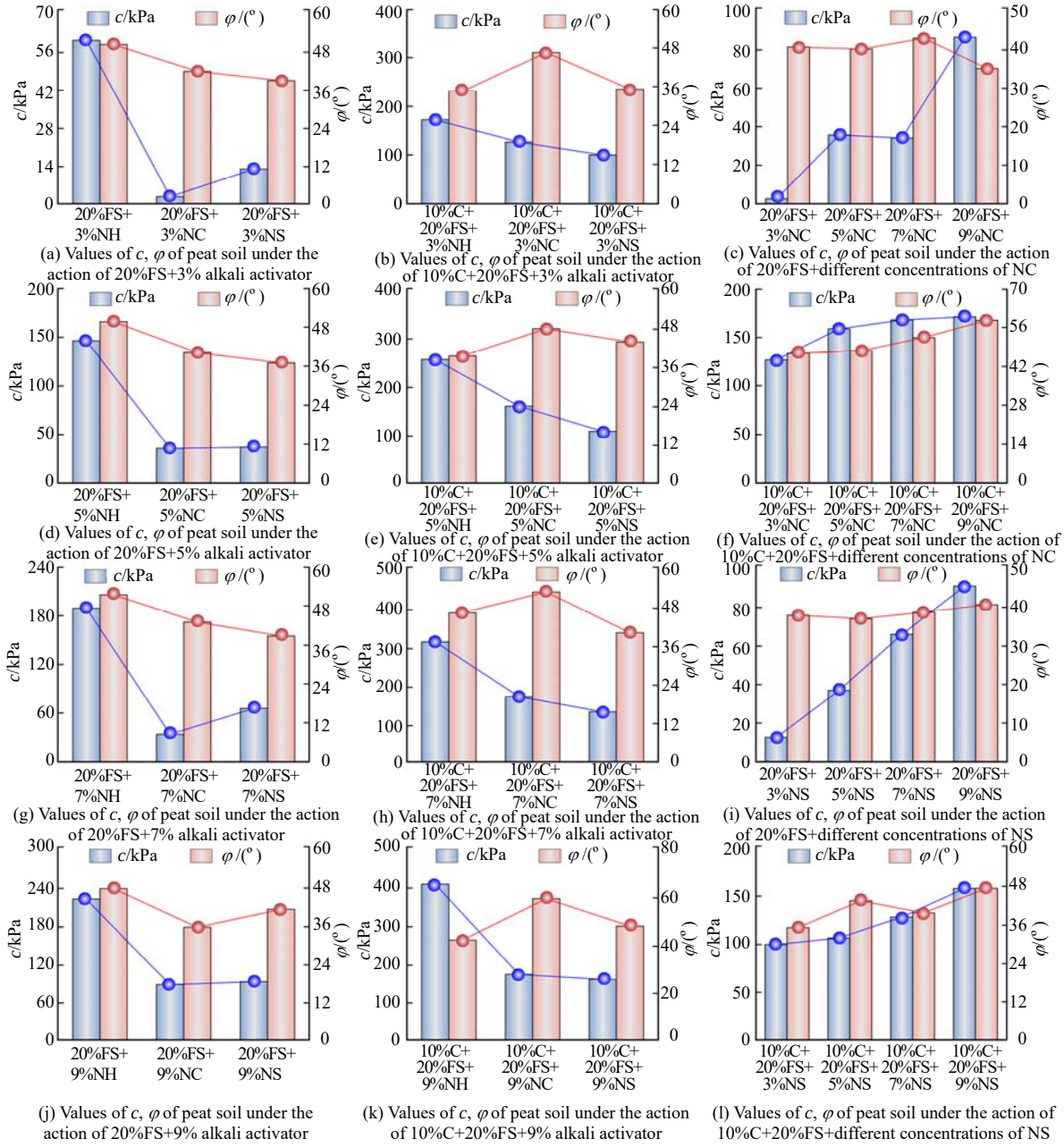

(a) Values of c, φ of peat soil under the action of 20%FS+3% alkali activator

(b) Values of c, φ of peat soil under the action of 10%C+20%FS+3% alkali activator

(c) Values of c, φ of peat soil under the action of 20%FS+different concentrations of NC

(d) Values of c, φ of peat soil under the action of 20%FS+5% alkali activator

(e) Values of c, φ of peat soil under the action of 10%C+20%FS+5% alkali activator

(f) Values of c, φ of peat soil under the action of 10%C+20%FS+different concentrations of NC

(g) Values of c, φ of peat soil under the action of 20%FS+7% alkali activator

(h) Values of c, φ of peat soil under the action of 10%C+20%FS+7% alkali activator

(i) Values of c, φ of peat soil under the action of 20%FS+different concentrations of NS

(j) Values of c, φ of peat soil under the action of 20%FS+9% alkali activator

(k) Values of c, φ of peat soil under the action of 10%C+20%FS+9% alkali activator

(l) Values of c, φ of peat soil under the action of 10%C+20%FS+different concentrations of NS

Fig. 11 Shear strength parameters (c and φ) of soil samples treated with different alkali activators

4 Discussion

4.1 Influence of mineral composition on peaty soil

The variations in the physical and mechanical properties of peaty soils are primarily attributed to changes in their mineral composition. Fig. 12 and 13 present the qualitative and quantitative analyses of the mineral compositions of untreated and modified soils, respectively. As shown in the figures, the dominant mineral components in the untreated soil are quartz, montmorillonite, muscovite, and trace amounts of kaolinite, with quartz comprising the highest proportion at approximately 55.3%, while the concentrations of other minerals remain relatively low[37]. Following cement addition, the quartz content decreased to 46.6%, while the amounts of montmorillonite and dolomite slightly increased. Meanwhile, C_3S and C_2S in the cement reacted with water to form hydrated calcium silicate (C-S-H) and calcium hydroxide ($Ca(OH)_2$), which subsequently filled the soil pore spaces, enhancing the soil's compactness[38]. The incorporation of 20% slag led to a reduction in quartz and montmorillonite contents, while muscovite content increased. Silicates and aluminates

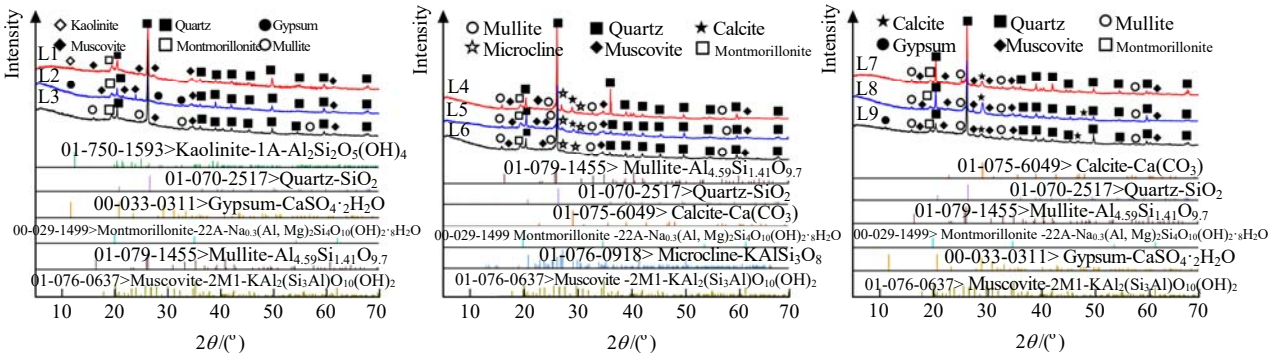

(a) Plain soil, soil mixed with 10%C, and soil mixed with 20%FS

(b) 20%FS+9% alkali activator

(c) 10%C+20%FS+9% alkali activator

Fig. 12 Qualitative analysis of the mineral composition of untreated and improved soils

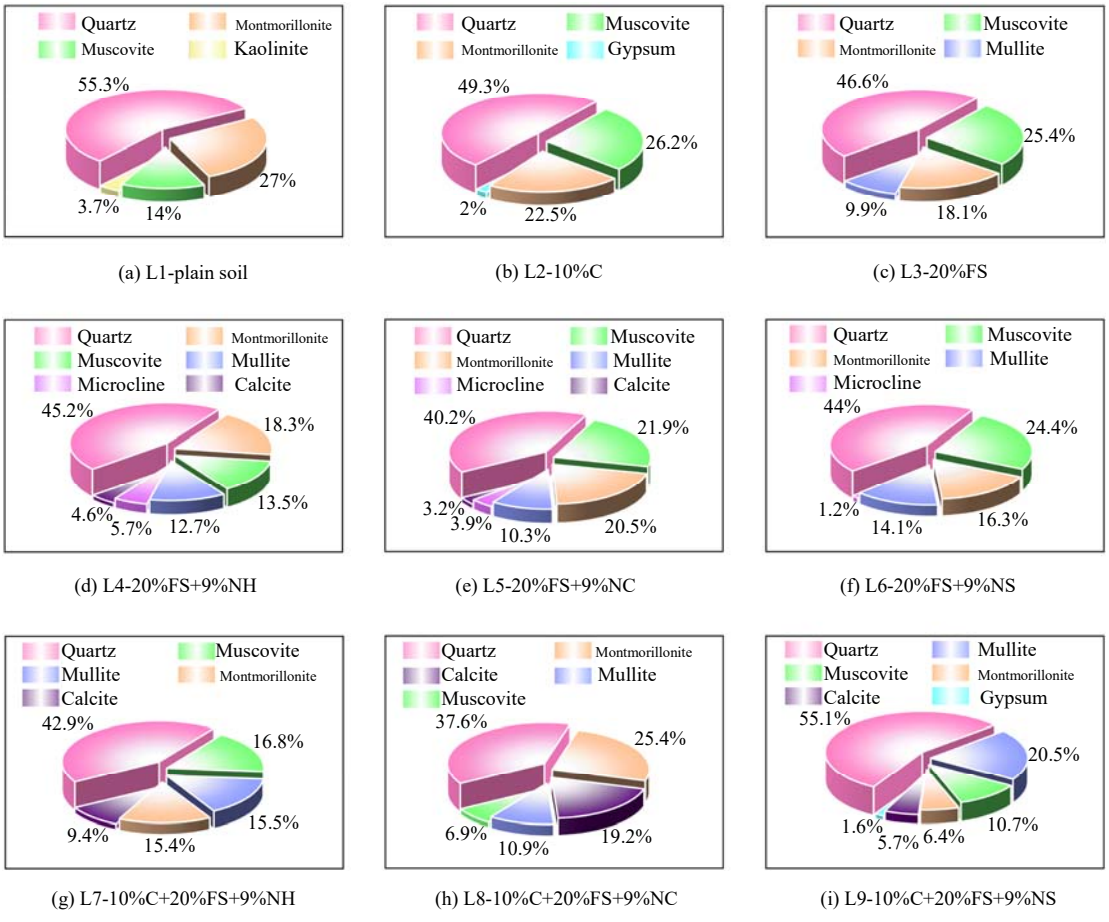

(a) L1-plain soil

(b) L2-10%C

(c) L3-20%FS

(d) L4-20%FS+9%NH

(e) L5-20%FS+9%NC

(f) L6-20%FS+9%NS

(g) L7-10%C+20%FS+9%NH

(h) L8-10%C+20%FS+9%NC

(i) L9-10%C+20%FS+9%NS

Fig. 13 Quantitative analysis of the mineral composition of untreated and improved soils

in the slag reacted with $Ca(OH)_2$ from the cement to form additional hydrated calcium silicate- aluminate (C-A-S-H) gels, thereby improving the structural stability of the soil.

The incorporation of an alkaline activator into the slag induced significant changes in the mineral composition of the peat soil samples, and notably promoted the formation of mullite and calcite. The alkaline activator accelerated the dissolution of Si, Al, and Ca ions from the slag[39], which then reacted with $Ca(OH)_2$ produced by the cement to form additional C-A-S-H gels, along with mullite and calcite. Under alkaline conditions, Si and Al from the slag dissolved and activated, forming a monolithic structure that crystallized with K^+ ions derived from both the soil and slag, ultimately yielding potassium feldspar crystals. As a rigid crystalline mineral, potassium feldspar has higher stability and lower solubility compared with the gel phase; it fills the soil pores and thus significantly improves the skeletal integrity and deformation resistance of the peat soil. The incorporation of cement into the alkali-activated slag system further increased the content of mullite and calcite in the soil samples. This enhancement resulted from the synergistic reactions among the cement, slag, and alkali activator, which produced additional hydration products and further improved the compressive and shear strength of the soil.

4.2 Impact of microstructural changes on peaty soil

The improvement in the mechanical strength of peaty soils reflects changes in their internal microstructure, including modifications in particle contact patterns[40]. SEM observations (Fig. 14 and Fig. 15) showed that the natural peaty soils had a relatively loose structure, with large pores and weak interparticle connections. After the addition of slag and an alkali activator, silicates and aluminates in the slag dissolved and reacted with $Ca(OH)_2$ under alkaline conditions to produce hydration products such as C-A-S-H gels and calomel. These products acted as binding agents between soil particles, effectively filling pore spaces and promoting the formation of agglomerates[41]. When cement was co-blended with slag and an alkali activator, the $Ca(OH)_2$ from the cement further enhanced the formation of C-A-S-H gels, while the silicates and aluminates accelerated agglomerate development. The formation of agglomerates compacted the soil matrix by establishing a rigid skeletal framework and filling pore spaces, thereby improving both the compressive strength and overall stability of the soil.

To investigate the microscopic pore structure characteristics of soil at multiple scales, SEM images magnified at 5.0k were selected. PCAS software was used for quantitative analysis of the microstructure of the modified soil[42]. First, the grayscale SEM images were binarized and noise was removed. An improved algorithm then achieved precise segmentation of particles and pores, with different mineral phases and soil particle pore distributions identified through color coding. Finally, vectorization was used to extract geometric parameters (e.g., particle and pore counts, areas, aspect ratios, shape factors), yielding statistical metrics such as porosity, fractal dimension, and area probability distribution indices. The oriented distribution characteristics were visualized through rose

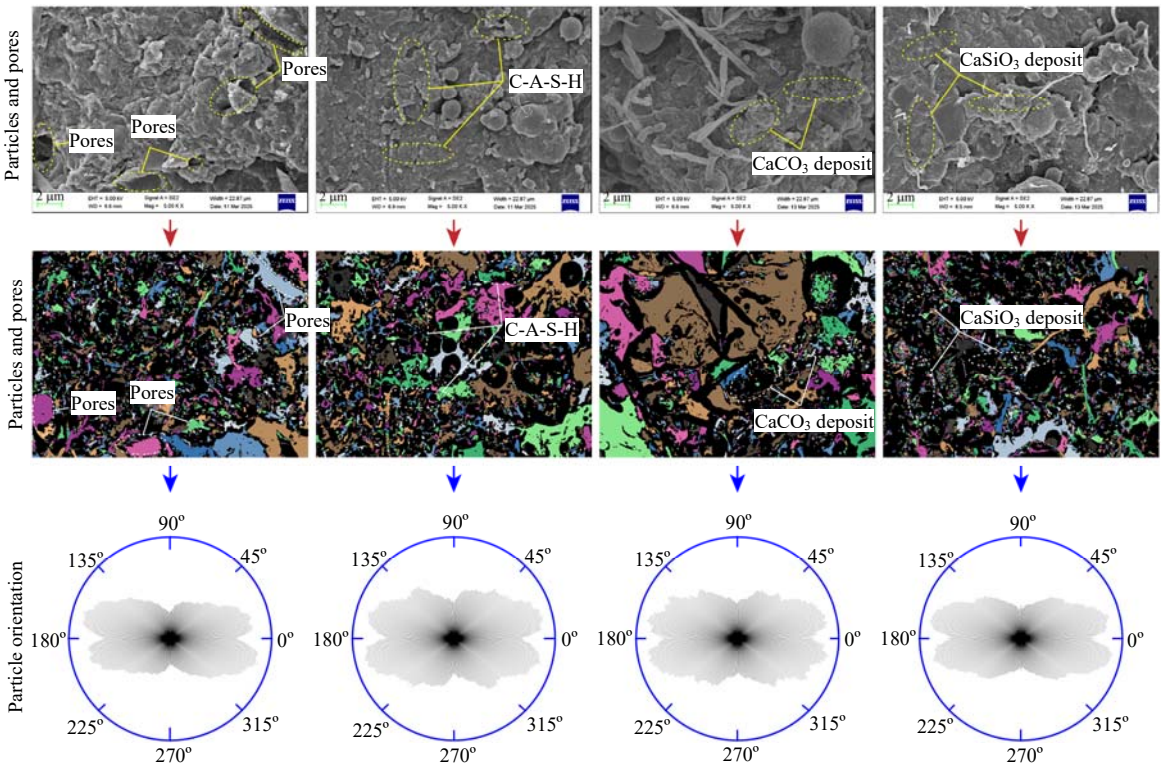

Fig. 14 SEM images of the mixture of slag and alkali activator

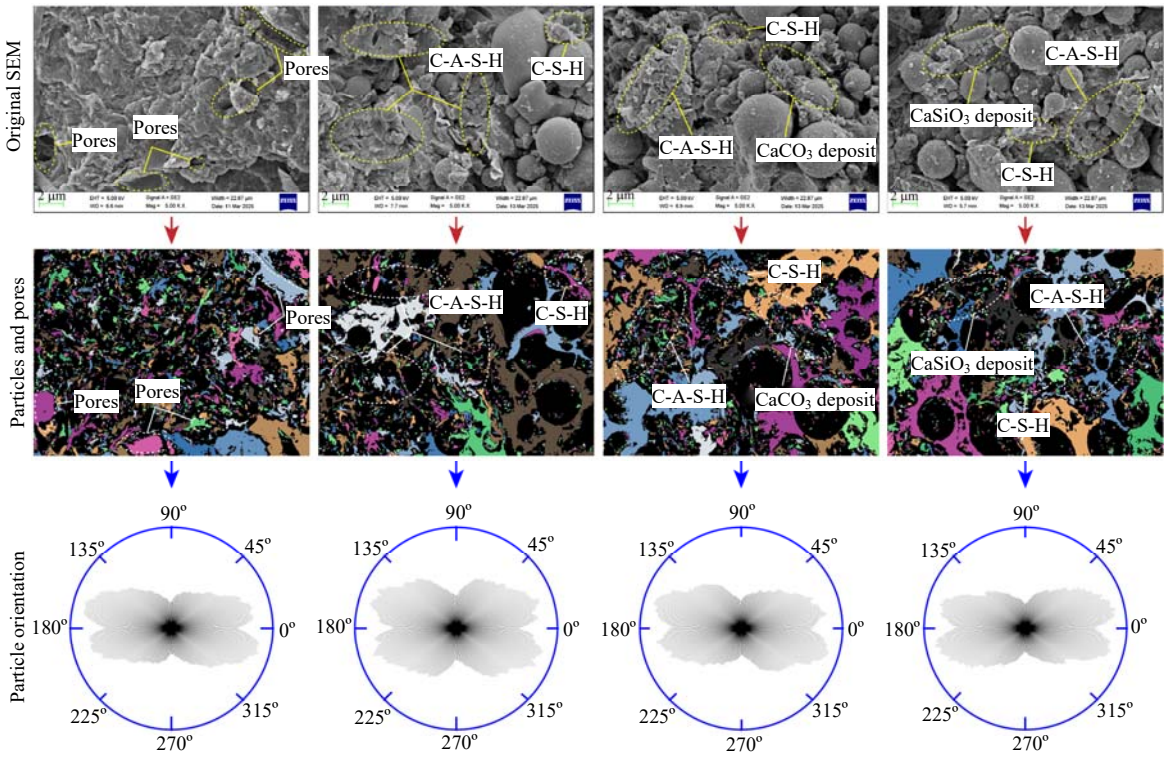

Fig. 15 SEM images of the mixture of cement, slag, and alkali activator

diagrams. The wind rose diagram of the natural peaty soil revealed a more dispersed particle distribution, indicating weaker interparticle bonding and higher overall porosity. After the addition of amendments, the soil exhibited a denser, more homogeneous particle arrangement, attributed to improved particle connectivity within the soil matrix, thereby enhancing its compactness. To further elucidate the relationship between macroscopic properties and microstructural characteristics, the grey correlation method was employed to quantify correlations between micro-structural parameters and mechanical behavior[43] (Fig. 16).

As shown in Fig. 16(a), pore area exhibited the strongest correlation with compressive strength, indicating that the morphology and spatial arrangement of soil particles significantly influence compressive performance. The strong correlations of pore length, width, and perimeter with compressive strength further suggest a direct relationship between pore geometry and soil bearing capacity. This aligns with micro-soil mechanics theory, which posits that larger pores reduce compressive per-formance, whereas smaller pores enhance load-bearing capacity. As illustrated in Fig. 16(b), the shape factor showed the highest correlation with shear strength, suggesting that particle morphology and spatial distribution play a decisive role in determining the soil's shear capacity[44]. Pore length and width also strongly correlated with shear strength, as larger pore dimensions, particularly increased pore width, tend to reduce shear resistance. The combined use of cement and slag, activated by alkali, significantly improved the soil's mechanical strength by optimizing shape factor, pore length, and pore width. For compressive strength, the correlation order was as follows: pore area > shape factor > pore perimeter > pore width > pore length. For shear strength, the ranking was: shape factor > pore length > pore width > pore perimeter > pore area.

To investigate the influence of porosity and pore distribution on the mechanical strength of modified peaty soils, the microscopic pore structure of the treated samples was quantitatively characterized using the MIP test (Fig. 17). The porosity of the peaty soil decreased markedly following the incorporation of modified slag (Fig. 17(i)). This was primarily attributed to the formation of hydration products, including C-A-S-H gel and $Ca(OH)_2$, from the reaction of slag with alkali, which filled the originally large pores and enhanced interparticle bonding, thereby increasing the soil density and reducing its porosity. In addition, cement further reacts in the alkaline environment to produce additional hydration products[45], while simultaneously facilitating the dissolution of minerals present in both slag and cement. The pore size distribution of the soil underwent significant alterations following the incorporation of various amendments (Fig. 17(a), 17(b) and 17(c)). Notably, in the pore region below 10 nm, the cumulative pore volume of the treated soil increased, indicating the formation of finer pores within the soil matrix. Conversely, in larger pore regions, the cumulative pore volume decreased markedly in samples treated with cement and slag[46]. This was attributed to the filling of large pores in the original soil matrix with hydration products generated by the amendments, thereby enhancing the structural

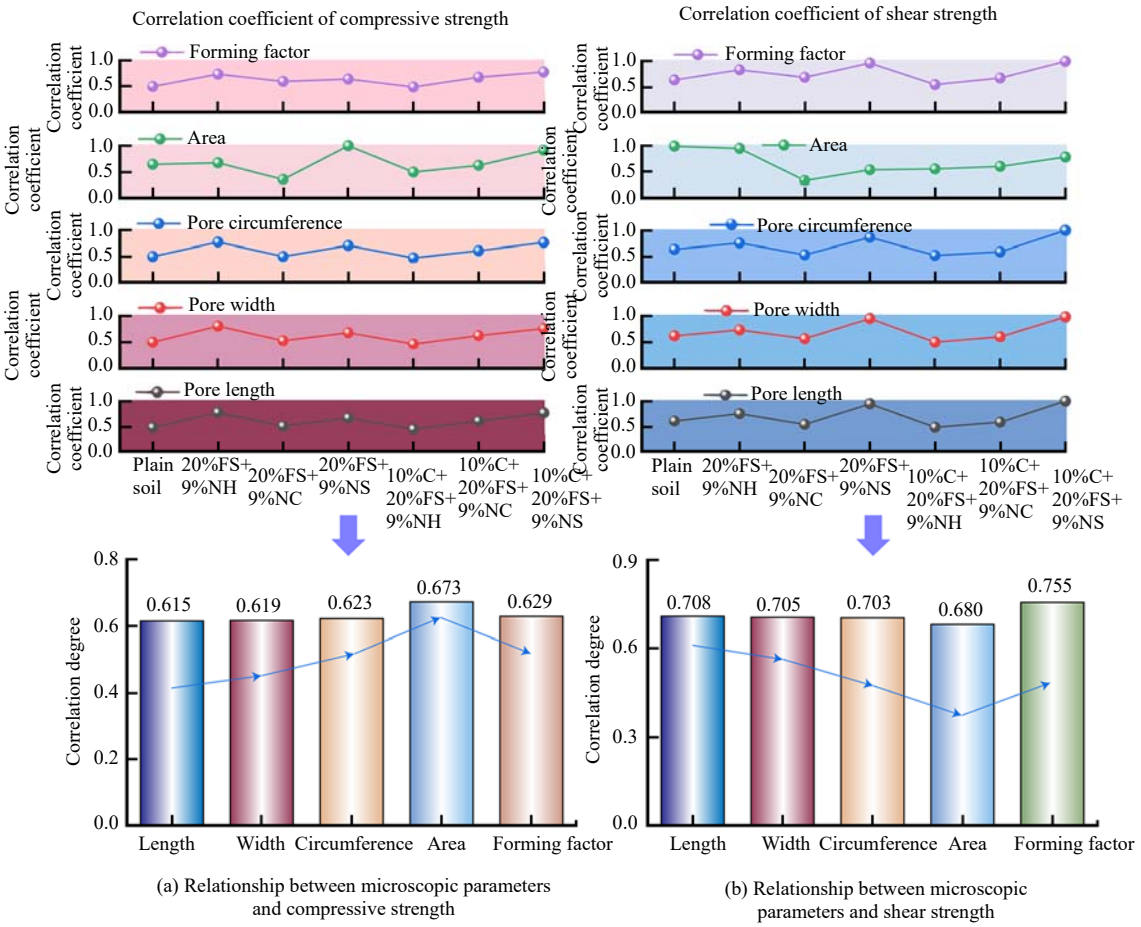

Fig. 16 Gray correlation diagrams

stability of the soil. Furthermore, the total pore volume and permeable pore volume of the soil decreased following alkali-activated treatment with cement and slag (Fig. 17(k), 17(l)), indicating a denser soil structure and reduced pore connectivity[47]. Differential porosity curves (Fig. 17(e), 17(f), 17(g)) further revealed that pore size distribution became more uniform following the incorporation of cement and slag. In particular, within the macroporous region (> 50 nm), the differential porosity decreased significantly upon the addition of cement and slag, suggesting that the macropores were effectively filled by hydration products.

4.3 Effect of organic matter on peaty soil

Variations in organic matter content significantly influence the physico-mechanical properties of peaty soils, due to the substantial presence of plant residues and undecomposed organic materials, such as humus, within the soil matrix[48−49]. In this study, FTIR testing was employed to quantify the organic matter content in the treated peaty soils.

As shown in Fig. 18, the absorption peak corresponding to C-H stretching vibrations appears in the range of 2 848−2 922 cm^{-1}, representing the alkyl chains present in the soil organic matter. With the incorporation of amendments, the intensity of the C-H absorption peaks gradually declined, primarily due to crosslinking interactions between metal ions from cement and slag and the organic matter in the soil. This interaction reduced the alkyl group content, subsequently weakening the C-H absorption signals. The absorption peaks at 1 620 cm^{-1} and 1 029 cm^{-1} correspond to C=C and C-O-C functional groups, indicating the presence of olefinic and ether bonds, respectively. Following the addition of cement and slag, the generated hydration products reacted with the soil's organic matter, forming more stable mineral phases, which disrupted these organic chemical bonds and altered the corresponding absorption peak intensities. As the organic matter in the soil underwent transformation[50], exemplified by the reduction of functional groups such as C-H and C=C, the overall soil structure was progressively enhanced, leading to improved mechanical stability. This mechanism is consistent with the findings of Gui[51], who used microbial techniques to reduce the organic matter content in peaty soils, thereby enhancing their mechanical strength.

4.4 Acting mechanisms of modifiers

4.4.1 Mechanisms of cement action

4.4.1.1 Initial adsorption and ion exchange

During the amelioration process, Ca^{2+} from the cement participate in ion exchange reactions with organic acids (e.g., -COOH) present in the peaty soil[52], becoming adsorbed onto the surfaces of soil particles and displacing exchangeable ions within the soil matrix (Fig. 19(a)).

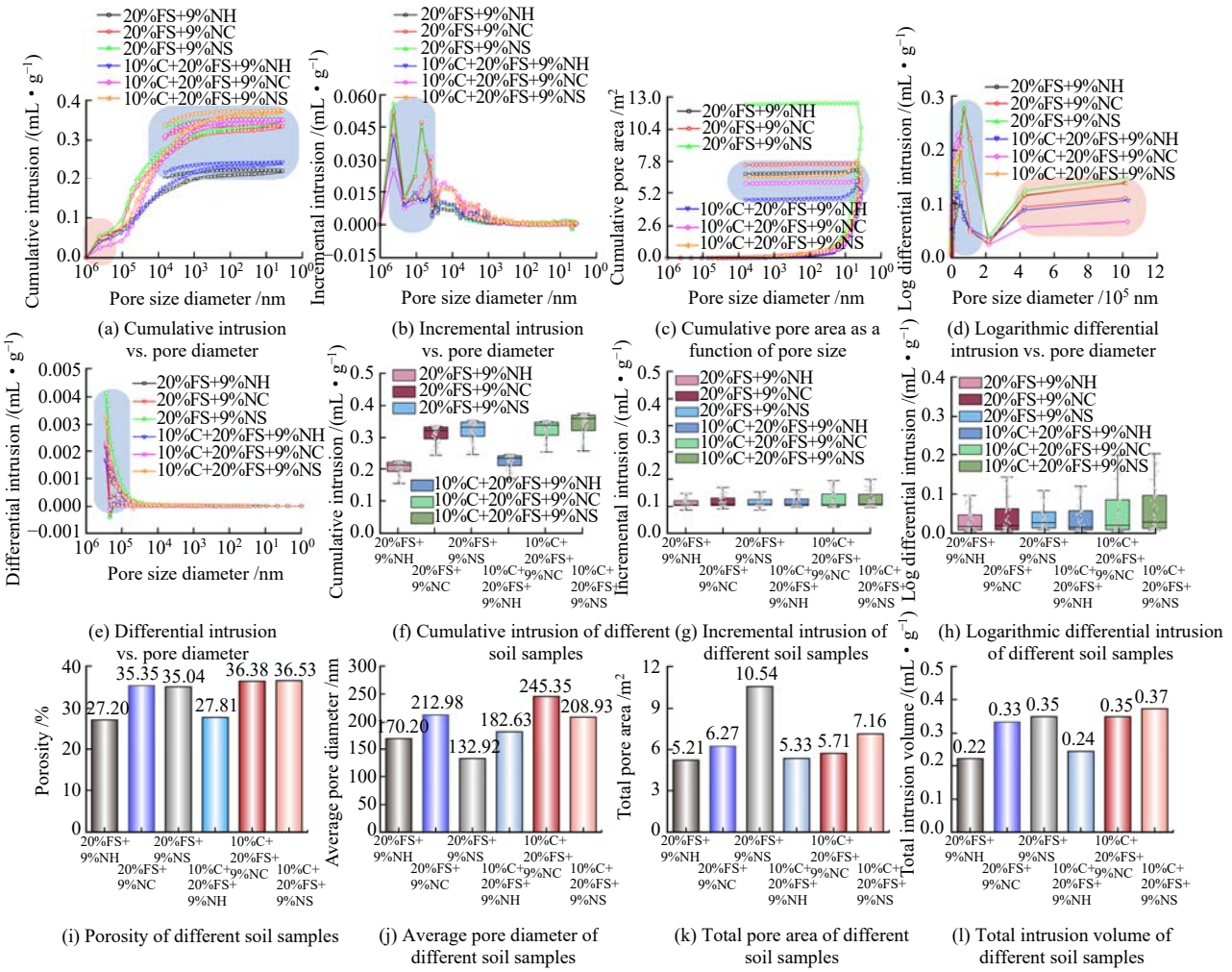

Fig. 17 Mercury intrusion porosimetry (MIP) results for soil samples

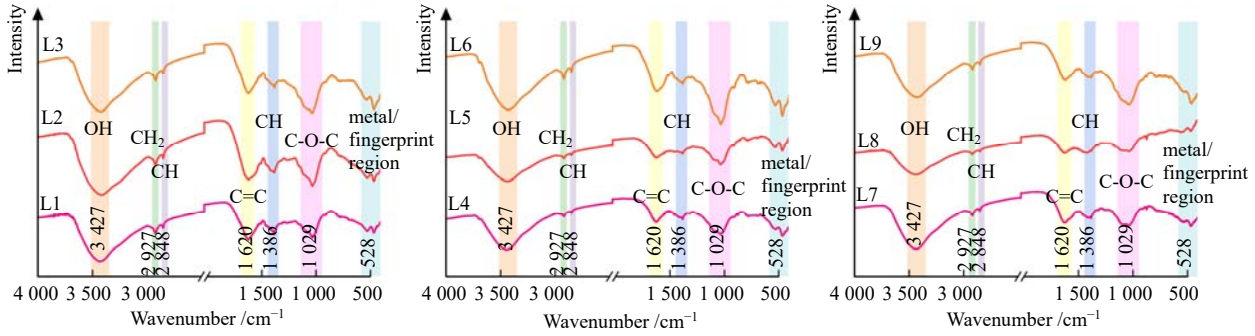

Fig. 18 Variation in organic matter content of soil samples

This ion exchange and initial adsorption process promotes the interaction between cement particles and soil, laying the groundwork for subsequent hydration reactions.

4.4.1.2 Formation of particle agglomeration

Hydration products of cement, such as $Ca(OH)_2$, gradually crystallize in alkaline environments and establish bridging interactions on the surfaces of soil particles (Fig. 19(b)). These bridging interactions promote the aggregation of soil particles and contribute to the development of a denser soil structure by strengthening interparticle bonding[53]. Consequently, soil particles aggregate into larger agglomerates, thereby improving the overall structural stability of the soil matrix.

4.4.1.3 Formation of stable carbonate structure

Ca^{2+} released from the cement reacts with atmospheric CO_2 to form stable $CaCO_3$. The formation of $CaCO_3$ not only enhances the hardness of the soil but also fills pore spaces[54], resulting in a denser soil structure (Fig. 19(c)).

Additionally, the presence of $CaCO_3$ improves the overall strength of the soil, particularly under loading conditions, and significantly enhances its compressive and shear strength.

4.4.1.4 Long-term development of strength

A portion of the hydration products generated by cement, primarily C-S-H gel, infiltrates the pores between soil particles and establishes a robust skeletal framework. The C-S-H gel subsequently encapsulates the surfaces of soil particles[54], thereby further enhancing the structural integrity of the soil matrix (Fig. 19(d)). As a result, this process reduces soil porosity, increases soil density, and significantly improves resistance to both compression and deformation.

4.4.1.5 Stress Action during Shearing

During the application of shear force, the friction between soil particles primarily resulted from the combined presence of C-S-H gel and $CaCO_3$, both of which effectively enhanced the soil's shear strength. The hydration products generated by cement contributed additional bonding forces, resisting external stresses and further increasing the soil's shear strength (Fig. 19(e)). SEM observations revealed that the surfaces of the treated soil particles were coated with C-S-H gel, which formed a structural skeleton (Fig. 19(f)). Additionally, $CaCO_3$ was observed filling both the surfaces of soil particles and the pore spaces, thereby further improving the strength and structural stability of the soil.

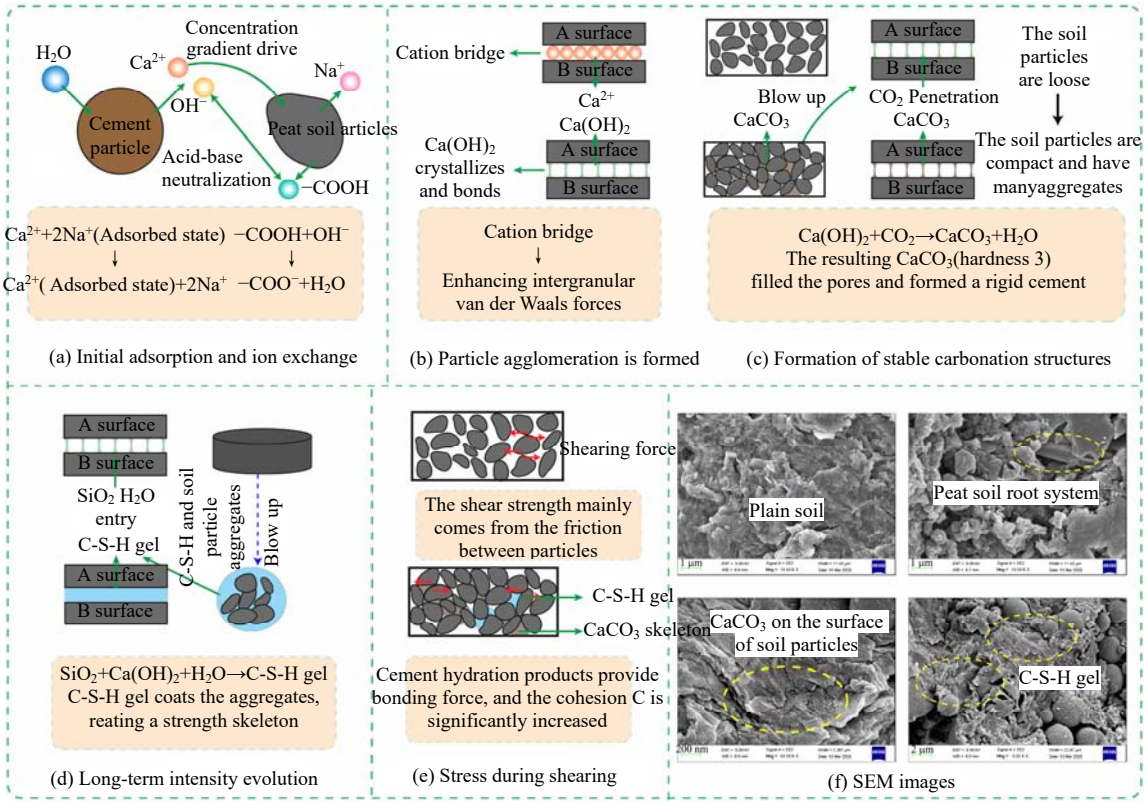

Fig. 19 Micro-mechanisms of peaty soils treated with cement

4.4.2 Mechanisms of modified slag action

When slag is applied to stabilize peaty soil in the presence of an alkali activator, the chemical reaction process within the curing system primarily involves four sequential stages: dissolution activation, ion exchange, gel formation, and structural reconstruction, ultimately resulting in the formation of a stable agglomerated structure and the enhancement of the soil's mechanical properties[55−56]. The specific process is described as follows:

Activation of slag properties by alkali activators. In the presence of alkali activators (NaOH, Na_2CO_3, and Na_2SiO_3), the vitreous phase within the slag was progressively dissolved by OH^-, breaking the original amorphous Si-O-Si and Al-O-Al bonds and releasing a substantial quantity of reactive ions, including SiO_4^{2-}, AlO_2^-, and Ca^{2+} (Fig. 20(a)). These released ions subsequently undergo condensation reactions in the alkaline environment, forming C-A-S-H gel characterized by a three-dimensional backbone structure[57]. Furthermore, in the presence of alkali activators, the surface reactions of slag particles gradually progress inward, reducing particle size, generating additional active sites, and accelerating the overall reaction rate. The resulting finer particles readily adhere to the surfaces of peat soil particles, effectively filling larger soil pores.

Ion exchange and adsorption processes. The intrinsic functional groups, including -COOH and -OH, in peaty

soils readily adsorb cations such as Ca^{2+} and Na^{+}, forming adsorption complexes that facilitate the precipitation and encapsulation of C-A-S-H gels on the surfaces of soil particles (Fig. 20(b)). Additionally, Na^{+} and SiO_3^{2-} supplied by Na_2SiO_3, together with the adsorbed Ca^{2+} in the soil, undergo cation exchange reactions to form $CaSiO_3$ precipitates, which contribute to pore filling and structural reinforcement; simultaneously, -COOH groups on the surface of organic matter in the peaty soil also participate in cation exchange, whereby Ca^{2+} replaces H^{+} or Na^{+} and adsorbs onto the surfaces, promoting the precipitation and encapsulation of C-A-S-H gels around the soil particles[58]. Meanwhile, -COOH groups on the surface of peat soil organic matter engage in cation exchange, with Ca^{2+} replacing H^{+} or Na^{+} and adsorbing onto the surface to form "calcium bridges" that enhance interparticle bonding. These reactions effectively passivate organic matter activity and lead to the formation of a stable organic-inorganic composite cluster structure.

Formation of dense structure of soil. The generated C-A-S-H gel eventually precipitates onto the surfaces of soil particles, filling the pores and encapsulating organic matter to form cementitious bridges (Fig. 20(c)). This process establishes a cohesive network among the particles, transforming the soil's internal framework from loosely packed particles into a densely bonded skeletal structure, thereby enhancing the initially weakly cemented nature of peaty soils. This structural transformation markedly decreases soil porosity, diminishes large pore spaces, and restrains the formation of microcracks. Simultaneously, it converts originally interconnected capillaries into closed or isolated micropores, thereby substantially enhancing the soil's compressive strength. Structural densification alters the primary source of soil shear resistance from interparticle friction to the combined effect of cementation and interparticle drag. Consequently, organic matter within the peaty soil remains physically protected from particle abrasion, preserving its integrity during mechanical loading. The organic matter in peaty soil does not undergo complete reaction but is instead physically adsorbed and chemically bonded to the C-A-S-H gel, forming an "organic matter-mineral-gel" composite. This composite reinforces the structural cohesion and consequently enhances the soil's shear strength[59].

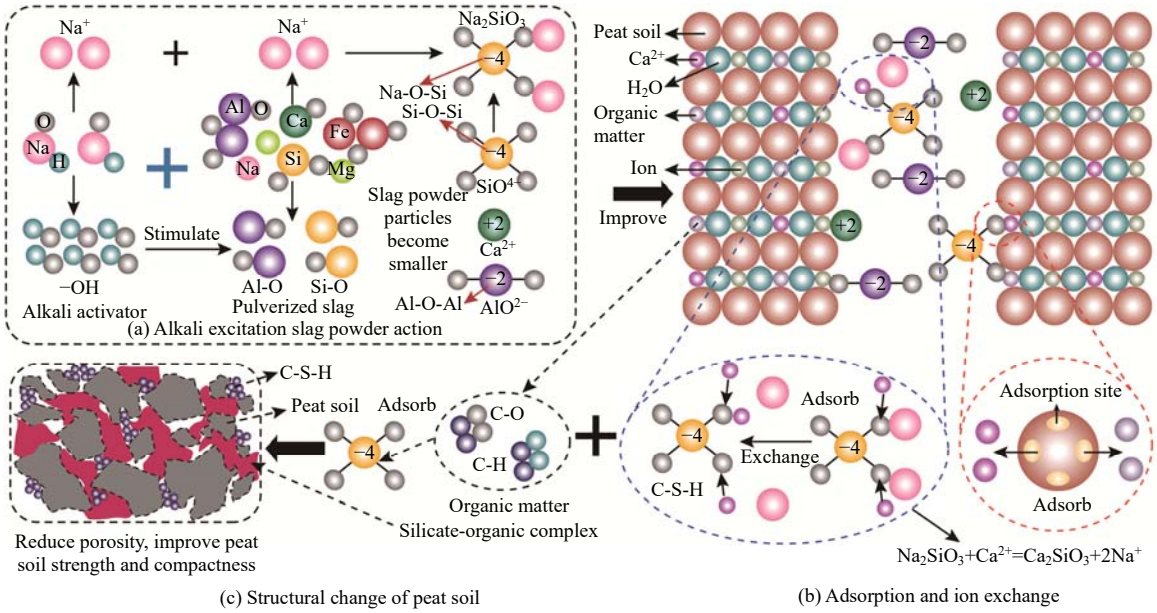

Fig. 20 Micro-mechanism of peaty soil stabilized with activated slag

4.5 Resistance to dry and wet conditions

To simulate the long-term evolution of soil properties during rainfall and evaporation under natural conditions, five freeze-thaw cycles were conducted on modified soil samples cured for 7 days[60]. Given the superior activation effect of NaOH, soil samples treated with NaOH were selected as examples. The modified soil samples reached a preliminary stable state after 20 minutes of immersion, establishing this duration as the immersion period. The samples were then removed from the water and dried in a 65 ℃ oven for 12 hours, completing one wet-dry cycle.

As shown in figure 21, the unconfined compressive strength of the soil sample gradually decreases with an increasing number of wet-dry cycles, eventually stabilizing. This change can be broadly divided into three stages: a rapid decline phase, a slow decay phase, and a strength stabilization phase[61]. NaOH concentration significantly influences strength retention. For example, when cement and slag were combined with 9% NaOH, the strength remained at 1 431 kPa after five freeze-thaw cycles, representing approximately 73% of the initial strength. In

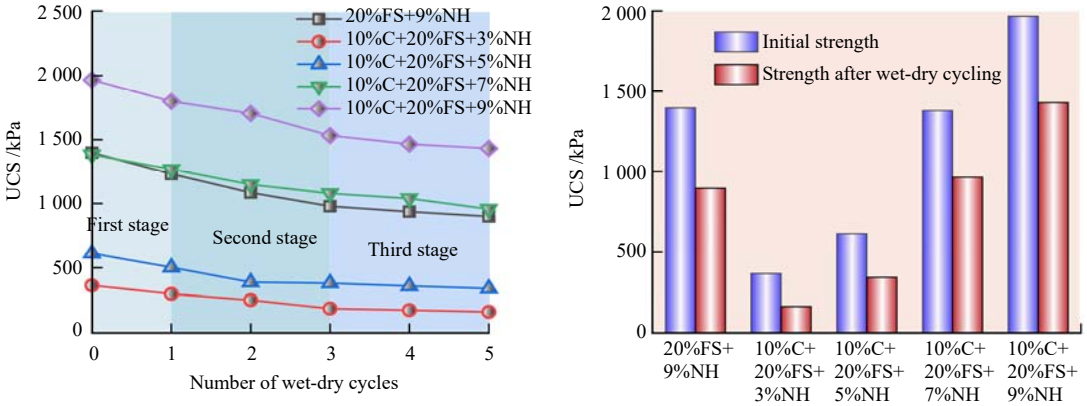

(a) Variation of compressive strength of soil samples with the number of wet-dry cycles

(b) Initial strength and post-cycle strength of soil samples

Fig. 21 Unconfined compressive strength of stabilized soil under wetting-drying cycles

contrast, at a lower NaOH concentration (3%), strength retention was only 44%. This demonstrates that higher activator dosages substantially enhance durability. Further comparison reveals that cement addition also affects strength retention. The initial strength of slag with only 9% NaOH was 1 398 kPa, which decreased to 895 kPa after five wet-dry cycles, corresponding to a strength loss of approximately 36%. In contrast, under the same conditions, the sample with 10% cement addition exhibited an initial strength of 1 967 kPa, retaining 1 431 kPa after cycles, resulting in a strength loss of only 27%. This indicates that the synergistic cementing effect between cement and alkali-activated slag promotes the formation of C-S-H and C-A-S-H gels, effectively filling pores and enhancing structural density.

Under cyclic loading, the strength evolution of modified soil samples is influenced by both the pore structure and the stability of cementation products[61]. During the initial stage of cycling, the strong hydrophilicity and weak cementation of organic matter in peaty soils cause the expansion of interfacial microcracks during water absorption and desorption, leading to rapid strength degradation. As cycling continues, cement hydration and alkali-activated reactions generate C-S-H and C-A-S-H gels, which progressively deposit, con- solidate, and form a stable spatial network, mitigating further strength loss. By the later stages of cycling, the system achieves internal densification and stability, maintaining strength at a residual level and exhibiting excellent durability. This process illustrates the structural optimization and long-term stabilization of peaty soils under the synergistic action of cement and alkali-activated slag.

5 Conclusions

This study examined the mechanical performance of modified peat soils through unconfined compressive strength and direct shear tests, complemented by microstructural analyses including SEM and XRD. The durability of the stabilized soils was further assessed under freeze-thaw cycling, and the underlying improvement mechanisms were systematically elucidated. The key findings can be summarized as follows:

(1) The cement-slag-alkali system markedly improves the mechanical strength of solidified peat soils, with the optimal ratio of 10% cement, 20% slag, and 7% NaOH providing a favorable balance between strength and ductility. The activation behavior of slag varies with activator type and concentration. In the absence of cement, the activation efficiency at low concentrations (3% and 5%) is in the order of NaOH > Na_2SiO_3 > Na_2CO_3, whereas that at high concentrations (7% and 9%) is in the order of NaOH > Na_2CO_3 > Na_2SiO_3. In the presence of cement, Na_2CO_3 shows the greatest efficiency at low concentrations, while at higher con- centrations the trend becomes NaOH > Na_2CO_3 > Na_2SiO_3.

(2) In cement-modified peat soils, particle bonding is primarily enhanced through ion exchange between Ca^{2+} and organic acid anions in the peat soil. In alkaline conditions, hydration products crystallize to form bridging structures that strengthen intergranular cohesion. Meanwhile, Ca^{2+} reacts with atmospheric CO_2 to form $CaCO_3$ precipitates, which increases the soil hardness and fills the soil pores. The generation of C-S-H gel further reduces porosity and, together with $CaCO_3$, forms a structural framework that increases intergranular friction and improves shear strength.

(3) The chemical process by which activated slag improves peat soils can be divided into four stages: dissolution activation, ion exchange, gel formation, and structural reorganization, ultimately producing a stable aggregate structure that enhances soil strength. Alkaline activators dissolve the vitreous phase of slag, releasing reactive ions that undergo polycondensation in alkaline conditions to form C-A-S-H gel. Organic functional groups in peat soils adsorb cations, driving ion exchange that generates $CaSiO_3$ precipitates and forms “calcium bridges.” The C-A-S-H gel then interacts with organic matter to create a dense “organic-mineral-gel” composite

matrix, reducing porosity, strengthening particle bonding, and thereby improving mechanical properties.

(4) The strength evolution of modified peat soil under wet-dry cycling proceeds through three stages: rapid decline, gradual attenuation, and stabilization. The synergistic cementation of cement and alkali-activated slag promotes gel formation that fills pores, increasing structural compactness and thereby reducing strength loss.

(5) Grey relational analysis was applied to quantify the relationship between microstructure and macroscopic mechanical properties. For compressive strength, the correlation ranked as: pore area > shape factor > pore perimeter > pore width > pore length; for shear strength, the order was: shape factor > pore length > pore width > pore perimeter > pore area.

CRediT authorship contribution statement

Yinlei Sun: Conceptualization, Writing – review & editing. **Lei Liao:** Writing – review & editing, Writing– original draft, Visualization, Methodology, Formal analysis, Data curation. **Xi Zou:** Conceptualization, Visualization. **Yanhua Zhou**: Conceptualization, Visualization. **Yun Cheng**: Conceptualization, Visualization. **Yunhao Guo:** Conceptualization, Visualization**. Zhiliang Wang**: Writing – review & editing, Formal analysis. **Xianwei Zhang:** Writing– review & editing, Formal analysis.

Declarations

Conflicts of interest All authors certify that they have no affiliations with or involvement in any organization or entity with any financial interest or non-financial interest in the subject matter or materials discussed in this manuscript.

Data Availability Statement

The author confirms that the data supporting the findings of this study are available within the article.

References

[1] LI W, O′KELLY B C, YANG M, et al. Compressibility behaviour and properties of peaty soils from Dianchi Lake area, China[J]. Engineering Geology, 2020, 277: 105778.

[2] LI X, YANG M, LI W, et al. Experimental investigation of consolidated undrained shear behavior on peaty soil in Dianchi, China[J]. Sustainability, 2022, 14(21): 14618.

[3] XUE Yuan, CUI Wei-xiu, FENG Zhi-jun, et al. The reinforcement technology of railway's soft soil foundation in Dian Lake area[J]. Journal of Railway Engineering Society, 2015, 32(8): 35−40.

[4] DING Zu-de, FU Jiang, LI Xi-song, et al. Properties of physical and mechanical indexes and correlation analysis of peaty soil in Kunming area[J]. Highway Engineering, 2018, 43(4): 86−91.

[5] RUAN Yong-fen, ZHU Shang-wan, ZHU Qiang, et al. Study on creep characteristics and model of plateau lacustrine peat soil[J]. Chinese Journal of Underground Space and Engineering, 2022, 18(3): 779−787.

[6] KAMARUIDZAMAN N S, ABU TALIB M K, ALIAS N A, et al. Peat stabilization by using sugarcane bagasse ash (SCBA) as a partial cement replacement materials[J]. International Journal of Integrated Engineering, 2019, 11(6): 204−213.

[7] ZAIDAN M N, ADNAN Z. Assessment of consolidation behavior for stabilized peat using cement and ceramic dust[J]. Recent Trends in Civil Engineering and Built Environment, 2022, 3(1): 1577−1585.

[8] KALANTARI B, PRASAD A. A study of the effect of various curing techniques on the strength of stabilized peat[J]. Transportation Geotechnics, 2014, 1(3): 119−128.

[9] RAHMAN N S S A. Effect of cement additive and curing period on some engineering properties of treated peat soil[J]. Sains Malaysiana, 2016, 45(11): 1679−1687.

[10] WONG L S, HASHIM R, ALI F. Utilization of sodium bentonite to maximize the filler and pozzolanic effects of stabilized peat[J]. Engineering Geology, 2013, 152(1): 56−66.

[11] LATIFI N, RASHID A S A, MARTO A, et al. Effect of magnesium chloride solution on the physico-chemical characteristics of tropical peat[J]. Environmental Earth Sciences, 2016, 75(3): 2−10.

[12] GUI Yue, WU Cheng-kun, ZHAO Zhen-xing, et al. Effects of microbial decomposition of organic matter on engineering properties of peat soil[J]. Rock and Soil Mechanics, 2020, 41(Suppl.1): 147−155.

[13] RUAN Yong-fen, YANG Bing, WU Long, et al. Mixture ratio design and application of chemically improved lake peat soil[J]. Bulletin of the Chinese Ceramic Society, 2021, 40(7): 2240−2247.

[14] CAO Jing, ZHANG Xing-wen, LEI Shu-yu, et al. Permeability of peat soil solidified by composite cement solidification agent[J]. Bulletin of the Chinese Ceramic Society, 2024, 43(10): 3561−3571.

[15] WANG Zhi-liang, MENG Hong-bin, SHEN Lin-fang, et al. Experimental study on artificially frozen peaty soil under the coupled heat-moisture-stress fields[J]. Chinese Journal of Underground Space and Engineering, 2022, 18(Suppl.2): 683−688, 695.

[16] GUO Yan-hui, MA Rui, MAO Shi-lin, et al. Test study on physical and mechanical properties of plateau bog phase peat soil[J]. Chinese Journal of Underground Space and

Engineering, 2024, 20(Suppl.1): 70−76.

[17] LI Lin, CAO Guang-zhu, ZHU Sai-nan. Experiment on improving mechanical character of Dianchi peat soil in Kunming[J]. Science Technology and Engineering, 2012, 12(11): 2768−2771.

[18] JIA Rui, CHU Zhen-xing. Research status and progress on solidifying soft clay by geopolymer[J]. Bulletin of the Chinese Ceramic Society, 2025, 44(2): 490−500.

[19] LURA P, LUNATI I, DESING H, et al. Mining the atmosphere: a concrete solution to global warming[J]. Resources, Conservation and Recycling, 2025, 212: 107968.

[20] YI Yao-lin, LI Chen, SUN Chuan, et al. Test on alkali-activated ground granulated blast-furnace slag(GGBS) for Lianyungang soft soil stabilization[J]. Chinese Journal of Rock Mechanics and Engineering, 2013, 32(9): 1820−1826.

[21] LIU Y, LU H, LIU M, et al. Microanalytical characterizations, mechanical strength and water resistance performance of solidified dredged sludge with industrial solid waste and architecture residue soil[J]. Case Studies in Construction Materials, 2022, 17: e01492.

[22] WANG D, WANG R, BENZERZOUR M, et al. Comparison between reactive MgO- and Na_2SO_4- activated low-calcium fly ash-solidified soils dredged from East Lake, China[J]. Marine Georesources and Geotechnology, 2020, 38(9): 1046−1055.

[23] LI S, WANG D, TANG C, et al. Optimization of synergy between cement, slag, and phosphogypsum for marine soft clay solidification[J]. Construction and Building Materials, 2023, 374: 130902.

[24] WANG D, XIAO J, HE F, et al. Durability evolution and associated micro-mechanisms of carbonated reactive MgO-fly ash solidified sludge from East Lake, China[J]. Construction and Building Materials, 2019, 208: 1−12.

[25] WU Jun, ZHENG Xi-yao, YANG Ai-wu, et al. Experimental study on the compressive strength of muddy clay solidified by the one-part slag-fly ash based geopolymer[J]. Rock and Soil Mechanics, 2021, 42(3): 647−655.

[26] FU S, WANG P, LIU S, et al. Treatment of waste marine clay by alkaline-activated ground granulated blast-furnace slag and municipal solid waste incineration bottom ash[J]. Journal of Rock Mechanics and Geotechnical Engineering, 2024, 17(5): 3243−3252.

[27] LIU X, BAO Y. Resource utilization strategy of kanbara reactor (KR) slag: oxidation desulfurization, material cycle, low-carbon green pathway[J]. Process Safety and Environmental Protection, 2025, 196: 106880.

[28] ZHAO Z, BENZERZOUR M, ABRIAK N, et al. Use of uncontaminated marine sediments in mortar and concrete by partial substitution of cement[J]. Cement and Concrete Composites, 2018, 93: 155−162.

[29] ZENTAR R, WANG D, ABRIAK N E, et al. Utilization of siliceous–aluminous fly ash and cement for solidification of marine sediments[J]. Construction and Building Materials, 2012, 35: 856−863.

[30] YAO J L, QIU H J, HE H, et al. Application of a soft soil stabilized by composite geopolymer[J]. Journal of Performance of Constructed Facilities, 2021, 35(4): 04021018.

[31] SUN Jia-ying, WANG Zhi-xin, DAI Ya-ying, et al. The application of geopolymer grouting material in the treatment of road soft soil[J]. Journal of Railway Science and Engineering, 2005, 2(2): 62−65.

[32] PU S, XU B, CAI G, et al. Strongly acidic lead contaminated soil solidification/stabilization using metakaolin-modified fly ash phosphoric-based geopolymer[J]. Chemical Engineering Journal, 2024, 496: 154336.

[33] O′KELLY B C, SIVAKUMAR V. Water content determinations for peat and other organic soils using the oven-drying method[J]. Drying Technology, 2014, 32(6): 631−643.

[34] CONSOLI N C, VAZ FERREIRA P M, TANG C, et al. A unique relationship determining strength of silty/clayey soils–Portland cement mixes[J]. Soils and Foundations, 2016, 56(6): 1082−1088.

[35] SARIOSSEIRI F, MUHUNTHAN B. Effect of cement treatment on geotechnical properties of some Washington State soils[J]. Engineering Geology, 2009, 104(1-2): 119−125.

[36] BONAVETTI V, DONZA H, RAHHAL V, et al. Influence of initial curing on the properties of concrete containing limestone blended cement[J]. Cement and concrete research, 2000, 30(5): 703−708.

[37] LIU Wei, ZHAO Fu-yu, YANG Wen-hui, et al. Features and properties of peaty soil in Caohai section of Anning-Sonming line[J]. Chinese Journal of Geotechnical Engineering, 2013, 35(Suppl.2): 671−674.

[38] QU Jun-tong, LUAN Kai-yu, PU Jun-xiang, et al. Dynamic characteristics of cement-phosphogypsum improving peaty soil[J]. Bulletin of the Chinese Ceramic Society, 2023, 42(12): 4427−4437.

[39] CRISTELO N, GLENDINNING S, FERNANDES L, et al. Effect of calcium content on soil stabilization with alkaline activation[J]. Construction and Building Materials, 2012, 29: 167−174.

[40] HE Yuan-yuan, PENG Qi-lan, WANG Li, et al. Investigating pore characteristics and permeability of seasonally frozen turfy soil using multiple micro-test methods[J]. Rock and Soil Mechanics, 2025, 46(1): 110−122.

[41] LIU Ya-long, WANG Ping, WANG Jing-kuan. Formation and stability mechanism of soil aggregates: progress and prospect[J]. Acta Pedologica Sinica, 2023, 60(3): 627−643.

[42] LIU C, SHI B, ZHOU J, et al. Quantification and characterization of microporosity by image processing, geometric measurement and statistical methods: application on SEM images of clay materials[J]. Applied Clay Science, 2011, 54(1): 97−106.

[43] YU C, HE C, LI Z, et al. Disintegration characteristics and mechanism of red clay improved by steel slag powder[J]. Construction and Building Materials, 2024, 444: 137873.

[44] CAI Si, RUAN Yong-fen, LI Peng-fei, et al. Shear characteristics and microstructural changes of peat soil[J]. China Earthquake Engineering Journal, 2022, 44(6): 1366−1374.

[45] WAHAB N, ABU TALIB M K, ABD MALIK A K, et al. Effect of cement stabilized peat on strength, microstructure, and chemical analysis[J]. Physics and Chemistry of the Earth, 2023, 129: 103348.

[46] AHMAD A, SUTANTO M H, AHMAD N R, et al. Microstructural characterization of fibric peat stabilized with Portland cement and silica fume[J]. Materials, 2023, 16(1): 18.

[47] AZAM F A A, CHE OMAR R, ROSLAN R, et al. Mechanical behavior, compressibility, and microstructural analysis of problematic soil through a green soil stabilization approach[J]. Results in Engineering, 2024, 24: 103524.

[48] O′KELLY B C, PICHAN S P. Effects of decomposition on the compressibility of fibrous peat—a review[J]. Geomechanics and Geoengineering: an International Journal, 2013, 8(4): 286−296.

[49] CHEN H, WANG Q. The behaviour of organic matter in the process of soft soil stabilization using cement[J]. Bulletin of Engineering Geology and the Environment, 2006, 65(4): 445−448.

[50] WATTEZ T, PATAPY C, FROUIN L, et al. Interactions between alkali-activated ground granulated blast furnace slag and organic matter in soil stabilization/ solidification[J]. Transportation Geotechnics, 2021, 26: 100412.

[51] GUI Yue, WU Cheng-kun, LIU Ying-shen, et al. Improving engineering properties of peaty soil by biogeotechnology[J]. Chinese Journal of Geotechnical Engineering, 2020, 42(2): 269−278.

[52] SU Y, LUO B, LUO Z, et al. Mechanical characteristics and solidification mechanism of slag/fly ash-based geopolymer and cement solidified organic clay: a comparative study[J]. Journal of Building Engineering, 2023, 71: 106459.

[53] WANG Zhi-liang, WANG Jing-yu, SHEN Lin-fang, et al. Effect of red clay replacement on strength of cement stabilized peaty soil[J]. Journal of Building Materials, 2019, 22(1): 87−93.

[54] HAUASHDH A, RADIN MOHAMED R M S, JAILANI J, et al. Stabilization of peat soil using fly ash, bottom ash and Portland cement: soil improvement and coal ash waste reduction approach[J]. Earth and Environmental Science, 2020, 498: 12011.

[55] FAN L F, CHEN D K, ZHONG W L. Effects of slag and alkaline solution contents on bonding strength of geopolymer-concrete composites[J]. Construction and Building Materials, 2023, 406: 133391.

[56] SITHOLE N T, MASHIFANA T. Geosynthesis of building and construction materials through alkaline activation of granulated blast furnace slag[J]. Construction and Building Materials, 2020, 264: 120712.

[57] LEONG E, ERIKTIUS D T. Improvement of peaty soils with municipal solid waste fly ash[J]. Environmental Geotechnics, 2014, 1(4): 200−209.

[58] HAN X, JIANG N, JIN F, et al. Effects of biochar-amended alkali-activated slag on the stabilization of coral sand in coastal areas[J]. Journal of Rock Mechanics and Geotechnical Engineering, 2023, 15(3): 760−772.

[59] KHANDAY S A, HUSSAIN M, DAS A K. Stabilization of Indian peat using alkali-activated ground granulated blast furnace slag[J]. Bulletin of Engineering Geology and the Environment, 2021, 80(7): 5539−5551.

[60] CHEN Kang, LIU Xian-feng, JIANG Guan-lu, et al. Degradation on mechanical properties of lime-treated red mudstone fill material subjected to wetting-drying cycles[J]. Rock and Soil Mechanics, 2025, 46(1): 43−54.

[61] RIVERA J F, OROBIO A, CRISTELO N, et al. Fly ash-based geopolymer as A4 type soil stabilizer[J]. Transportation Geotechnics, 2020, 25: 100409.

[62] SARGENT P, HUGHES P N, ROUAINIA M. A new low carbon cementitious binder for stabilizing weak ground conditions through deep soil mixing[J]. Soils and Foundations, 2016, 56(6): 1021−1034.